Journal for ImmunoTherapy of Cancer

Small extracellular vesicles induce resistance to anti-GD2 immunotherapy unveiling tipifarnib as an adjunct to neuroblastoma immunotherapy

Xiaoming Liu,[1] Carson A Wills ,[1] Longgui Chen,[1] Jiawen Zhang,[1] Yuanjun Zhao,[2] Mi Zhou,[2] Jeffrey M Sundstrom,[2] Todd Schell,[3] Vladimir S Spiegelman,[1] Megan M Young,[1] Hong-Gang Wang[1]

To cite: Liu X, Wills CA, Chen L, *et al*. Small extracellular vesicles induce resistance to anti-GD2 immunotherapy unveiling tipifarnib as an adjunct to neuroblastoma immunotherapy. *Journal for ImmunoTherapy of Cancer* 2022;**10**:e004399. doi:10.1136/jitc-2021-004399

► Additional supplemental material is published online only. To view, please visit the journal online (http://dx.doi.org/10.1136/jitc-2021-004399).

XL and CAW contributed equally.

Accepted 23 March 2022

[1]Department of Pediatrics, The Pennsylvania State University College of Medicine, Hershey, Pennsylvania, USA
[2]Department of Ophthalmology, The Pennsylvania State University College of Medicine, Hershey, Pennsylvania, USA
[3]Microbiology and Immunology, The Pennsylvania State University College of Medicine, Hershey, Pennsylvania, USA

Correspondence to
Hong-Gang Wang;
hwang3@pennstatehealth.psu.edu

ABSTRACT

Background Anti-GD2 monoclonal antibody immunotherapy has significantly improved the overall survival rate for high-risk neuroblastoma patients. However, 40% of patients fail to respond or develop resistance to treatment, and the molecular mechanisms by which this occurs remain poorly understood. Tumor-derived small extracellular vesicles (sEVs) have emerged as critical regulators in modulating the response to immunotherapy. In this study, we investigated the role of neuroblastoma-derived sEVs in promoting resistance to the anti-GD2 monoclonal antibody dinutuximab. Moreover, to determine whether pharmacologic inhibition of sEV secretion sensitizes tumors to dinutuximab treatment, we combined dinutuximab with tipifarnib, a farnesyltransferase inhibitor that inhibits sEV secretion.

Methods We investigated the role of neuroblastoma-derived sEVs in modulating the response to dinutuximab by utilizing the syngeneic 9464D-GD2 mouse model. The effect of neuroblastoma-derived sEVs in modulating the tumor microenvironment (TME) and host immune system were evaluated by RNA-sequencing and flow cytometry. Importantly, we used this mouse model to investigate the efficacy of tipifarnib in sensitizing neuroblastoma tumors to dinutuximab. The effect of tipifarnib on both the TME and host immune system were assessed by flow cytometry.

Results We demonstrated that neuroblastoma-derived sEVs significantly attenuated the efficacy of dinutuximab *in vivo* and modulated tumor immune cell infiltration upon dinutuximab treatment to create an immunosuppressive TME that contains more tumor-associated macrophages and fewer tumor-infiltrating NK cells. In addition, we demonstrated that neuroblastoma-derived sEVs suppress splenic NK cell maturation *in vivo* and dinutuximab-induced NK cell-mediated antibody-dependent cellular cytotoxicity *in vitro*. Importantly, tipifarnib drastically enhanced the efficacy of dinutuximab-mediated inhibition of tumor growth and prevented the immunosuppressive effects of neuroblastoma-derived sEVs *in vivo*.

Conclusions These preclinical findings uncover a novel mechanism by which neuroblastoma-derived sEVs modulate the immune system to promote resistance to dinutuximab and suggest that tipifarnib-mediated inhibition of sEV secretion may serve as a viable treatment strategy to enhance the antitumor efficacy of anti-GD2 immunotherapy in high-risk neuroblastoma patients.

Key messages

What is already known on this topic

► Tumor-derived small extracellular vesicles (sEVs) have immunosuppressive functions and modulate the response to immunotherapy.

What this study adds

► This study identifies an immunosuppressive tumor microenvironment as a novel mechanism of resistance to anti-GD2 immunotherapy mediated by neuroblastoma-derived sEVs and identifies tipifarnib as a promising adjunct to dinutuximab, which could be translated to the clinic to improve patient outcomes.

INTRODUCTION

Neuroblastoma is the most common extracranial solid tumor in children, accounting for approximately 6% of all pediatric malignancies and more than 10% of childhood cancer-related deaths.[1] The standard treatment regimen for patients with high-risk neuroblastoma includes multiagent chemotherapy, surgery, autologous stem cell transplantation, radiotherapy, and maintenance therapy.[2] Despite multimodal treatment, the 5-year overall survival rate for patients with high-risk disease is only around 50%.[3]

The recent incorporation of dinutuximab and immunostimulatory agents (granulocyte-macrophage colony-stimulating factor and interleukin-2) into maintenance therapy for patients with high-risk neuroblastoma has substantially improved patient outcomes.[4] Dinutuximab (ch14.18) is a chimeric monoclonal antibody against the disialoganglioside

GD2, which is expressed on the outer leaflet of the plasma membrane of peripheral neurons, skin melanocytes, and the central nervous system, and is ubiquitously present on tumors of neuroectodermal origin, including most neuroblastomas.[5–7] Tumor-bound anti-GD2 antibodies recruit immune effector cells to trigger Fc-receptor-mediated killing by both complement-mediated cytotoxicity and antibody-dependent cell-mediated cytotoxicity (ADCC).[4] Due to the specificity of GD2 for tumors of neuroectodermal origin, recent studies have investigated the use of anti-GD2 CAR-NKT and CAR-T cell therapies for patients with refractory neuroblastoma.[8 9] However, despite its relative clinical success, more than 40% of neuroblastoma patients fail to respond or develop resistance to anti-GD2 therapy.[10] Moreover, although anti-GD2 immunotherapy is highly effective against minimal residual disease, it has limited efficacy for targeting solid tumors.[10] However, the mechanisms underlying therapeutic failure and resistance to anti-GD2 immunotherapy remain unknown.[10 11]

Small extracellular vesicles (sEVs) have recently emerged as critical regulators of tumor growth, metastasis and cancer progression.[12] These 30–150 nm vesicles are secreted by almost all cell types through outward budding of the plasma membrane or direct fusion of multivesicular bodies with the plasma membrane. Notably, sEVs contain biologically active molecules capable of modulating the extracellular environment and immune system.[13] Recent studies have found that tumor-derived sEVs play an important role in promoting resistance to immunotherapy by interacting with immune effector cells and suppressing the host immune system.[14 15] NK cells, which express the receptor FcgRIIIa (CD16), are the major effector cells for anti-GD2 immunotherapy and use ADCC to target neuroblastoma cells.[16] Tumor-derived sEVs attenuate ADCC in vitro by inhibiting the binding of antibodies to tumor cells.[17] Moreover, tumor-derived sEVs have been shown to dysregulate NK cell function and induce NK cell exhaustion.[18 19] However, whether tumor-derived sEVs regulate resistance to anti-GD2 monoclonal antibody immunotherapy *in vivo* remains unclear.

In this study, we use a well-characterized preclinical mouse model of neuroblastoma to reveal that neuroblastoma-derived sEVs induce resistance to anti-GD2 immunotherapy. We show that neuroblastoma-derived sEVs modulate the systemic immune response and alter tumor immune cell infiltration following dinutuximab treatment to establish an immunosuppressive TME and promote evasion of dinutuximab-induced cytotoxicity. Importantly, we identify tipifarnib, an FDA-approved farnesyltransferase inhibitor shown to inhibit sEV secretion, as a novel agent that enhances the efficacy of dinutuximab and prevents the development of sEV-induced immunosuppression. Taken together, our preclinical results provide a promising new treatment option that can be rapidly translated to the clinic to improve outcomes for high-risk neuroblastoma patients.

MATERIALS AND METHODS

Cell lines and plasmids

The mouse 9464D neuroblastoma cell line was a gift from Dr Paul Sondel (University of Wisconsin, Madison, Wisconsin, USA). Human IMR32 neuroblastoma (CCL-127), HEK 293T/17 (CRL-11268), and NK92-EGFP-CD16 (PTA-8836) cell lines were purchased from ATCC. Neuroblastoma and HEK 293T/17 cells were cultured in Dulbecco's Modified Eagle's Medium (DMEM; Corning, 10–013-CV) supplemented with 10% heat-inactivated fetal bovine serum (FBS) (Sigma-Aldrich F2442) and 1% antibiotic-antimycotic (Corning, 30–004 CI). NK-92-EGFP-CD16 cells were cultured in RPMI 1640 (Corning, 10–040-CV) containing 10% horse serum (Equitech-Bio, SE30-0100), 10% heat-inactivated FBS, and 100 units/mL IL-2 (BioLegend, 589104-BL). Cells were incubated at 37°C in a humidified chamber containing 5% CO_2. All cell lines used in this study were thawed from frozen stock and maintained in cell culture for less than 6 months. Cells were periodically authenticated by mycoplasma testing, morphologic inspection, and STR analysis.

The pCDH1-CMV-MCS-SV40-Hygro construct was previously described.[20] SFG.GD3 synthase (*St8sia1*)–2A-GD2 synthase (*B4galnt1*) was obtained from Martin Pule through Addgene (#75013). pCDH1-CMV-*St8sia1*-2A-*B4galnt1*-SV40-Hygro construct was generated by subcloning the PCR amplified (primer set: 5'- ATCC TCTAGACTGCCACCATGAG-3', 5'- TAAATTCGAATC ACTCGGCGGTCATGCACT-3') *St8sia1*-2A-*B4galnt1* cassette into the XbaI-BstBI site of pCDH1-CMV-MCS-SV40-Hygro. 9464D-GD2 cells were generated by transducing 9464D cells with lentiviral particles harboring pCDH1-CMV-*St8sia1*-2A-*B4galnt1*-SV40-Hygro followed by selection with hygromycin (400 µg/mL).

Drugs and antibodies

Dinutuximab (Unituxin®) was a gift from the Penn State Health Pharmacy (Hershey, Pennsylvania, USA). Tipifarnib (AdooQ, MedChemExpress) was dissolved in dimethylsulfoxide (DMSO) to create a 10 mM stock solution for *in vitro* use or suspended at 4 mg/mL in 20% w/v hydroxypropyl-β-cyclodextrin (Millipore Sigma, 3 32 607–100G) in distilled water, pH 2.5 for *in vivo* studies. The following antibodies were used for immunoblotting: Alix (Cell Signaling Technology, 3A9, 1:1000), CD63 (Abcam, ab217345, 1:1000), Calnexin (Abcam, ab22595, 1:1000), Tsg101 (GeneTex, 70255, 1:500), Rab27a (Cell Signaling Technology, 69 295S, 1:1000), β-Actin (Sigma, A5441, 1:10,000), and Golgin97 (Thermo Fisher, A-21270, 1:1000). Antibodies used for flow cytometry are included in online supplemental table S1.

Small extracellular vesicles (sEVs) were isolated from conditioned cell culture medium according to a previously described differential ultracentrifugation method.[21] Briefly, FBS was depleted of sEVs by centrifuging heat-inactivated FBS two times at 120,000 relative centrifugal force (RCF) for 12 hours at 4°C (Beckman, SW32Ti) followed by filtration of the supernatant through a

0.2 µm filter. Conditioned cell culture medium was collected from cells cultured for 24 hours in DMEM supplemented with 10% sEV-depleted FBS. The conditioned medium was centrifuged at 500 RCF for 10 min at 4°C (Beckman, SX4750A) to remove cells and large cell debris. The supernatant was filtered through a 0.2 µm syringe filter (VWR 28 145–501) and concentrated using a 100K molecular weight cutoff (MWCO) protein concentrator (Thermo Fisher, 88533). The concentrated supernatant was centrifuged at 10,000 RCF for 20 min at 4°C (Eppendorf, FA-45-30-11) to remove larger microvesicles and apoptotic bodies followed by centrifugation at 120,000 RCF for 4 hours at 4°C (Beckman, SW55Ti). The sEV-containing pellet was washed two times in ice-cold phosphate-buffered saline (PBS) and pelleted by centrifugation at 120,000 RCF at 4°C for 4 hours and 12 hours, respectively (Beckman, SW55Ti). The sEV-containing pellet was resuspended in PBS and stored at −20°C.

Animal experiments

All animal studies were performed according to guidelines established by the Institutional Animal Care and Use Committee (IACUC #PRAM201145989) at the Penn State College of Medicine (Hershey, Pennsylvania, USA). An immunocompetent mouse model of neuroblastoma was generated by subcutaneously injecting 1×10^6 9464D-GD2 cells in a 50:50 mixture of DMEM and Matrigel (Corning, 354234) into C57BL/6J mice (8–10-week-old, JAX 000664) with male and female mice represented at an equal ratio. One week following tumor cell inoculation, mice were randomized into treatment groups. Where indicated, mice were treated two times per week by tail-vein injection with PBS (100 µL), dinutuximab (25 µg in 100 µL PBS), purified sEVs from 9464D-GD2 cells (20 µg in 100 µL PBS), or the combination of dinutuximab and sEVs. Where indicated, tipifarnib (25 mg/kg) or an equivalent volume of vehicle was administered two times a day by oral gavage. Primary tumor growth was monitored by measuring tumor volume using calipers (volume = π(length*width^2/6). At the experimental endpoint, mice were euthanized, and tumor, blood, spleen, and bone marrow (BM) were harvested for ex vivo analysis. Endpoint tumor volume was calculated by measuring tumors using calipers (volume = π(length*width*height)/6).

Flow cytometry

For cell surface staining, approximately 1×10^6 cells were stained with pre-mixed antibody cocktail panels (online supplemental table S1) in 100 µL fluorescence-activated cell sorting (FACS) buffer (1% FBS, 0.2% NaN_3 in PBS) for 30 min on ice. Cells were washed two times with FACS buffer and fixed with 2% paraformaldehyde (Fisher Scientific, 50-980-487) for 15 min. Fixed cells were washed once with PBS and resuspended in 0.5 mL FACS buffer for flow cytometric analysis using an LSR II or Symphony flow cytometer (BD Biosciences). Compensation was performed using UltraComp eBeads™ compensation beads (Invitrogen). FlowJo v10 (FlowJo, LLC) software was used for data analysis.

In vitro NK cell-mediated ADCC assay

The coculture assay was adapted and modified from Barry *et al*.[22] Briefly, neuroblastoma cells were seeded at 2×10^4 cells per well in a 96-well plate. The following day, the medium was removed, cells were washed in PBS, and 1×10^4 NK92-CD16-EGFP cells (effector:target ratio of 1:2) were added in RPMI 1640 containing 10% FBS, 100 units/mL IL2, and 0.5 µM YOYO-3 iodide (ThermoFisher, Y3606). Where indicated, NK92-CD16-EGFP cells were preincubated with neuroblastoma-derived sEVs (25 µg/mL) for 2 hours prior to addition, and dinutuximab was added to the co-culture at a concentration of 100 ng/mL. Images were taken at 1-hour intervals using the Incucyte S3 Live Cell Imaging System (Sartorius) and quantified using the Incucyte Cell-by-Cell Analysis Software Module (Sartorius).

Statistical analysis

GraphPad Prism (GraphPad Software) was used for statistical analysis. Two-tailed unpaired student t-tests were used for single comparisons. One-way analysis of variance with Tukey's/Sidak's posthoc tests were used for multiple comparisons. Statistical significance was set to $p<0.05$.

RESULTS

Neuroblastoma-derived sEVs promote resistance to dinutuximab in vivo

The 9464D cell line is derived from a spontaneous neuroblastoma that arose in a TH-MYCN transgenic mouse on the C57BL/6 background, creating a genetically defined transplantable tumor model.[23 24] While the complex, acidic ganglioside GD2 is highly expressed on most neuroblastoma, 9464D cells express a lower cell surface level of GD2 compared with other neuroblastoma cell lines.[24 25] To establish a syngeneic model of neuroblastoma suitable for investigating mechanisms of resistance to anti-GD2 immunotherapy, murine GD3 synthase (*St8sia1*), the rate-limiting enzyme for GD2 biosynthesis, and GM2/GD2 synthase (*B4galnt1*) were stably overexpressed in 9464D cells to upregulate cell surface GD2 expression (9464D-GD2; online supplemental figure S1A). sEVs were isolated from 9464D-GD2 cells using a well-established differential ultracentrifugation protocol[21] (online supplemental figure S1B) and were found to demonstrate the characteristic morphology, protein markers, and size distribution of sEVs (figure 1A–C).[26] To determine how sEVs regulate tumor growth and resistance to anti-GD2 immunotherapy *in vivo*, immunocompetent C57BL/6 mice were subcutaneously inoculated with 1×10^6 9464D-GD2 cells. One-week post-inoculation, tumor-bearing mice began receiving two times per week tail-vein injections of PBS, dinutuximab, and/or sEVs isolated from 9464D-GD2 cells (hereafter denoted sEVs unless otherwise noted) and were monitored for tumor growth

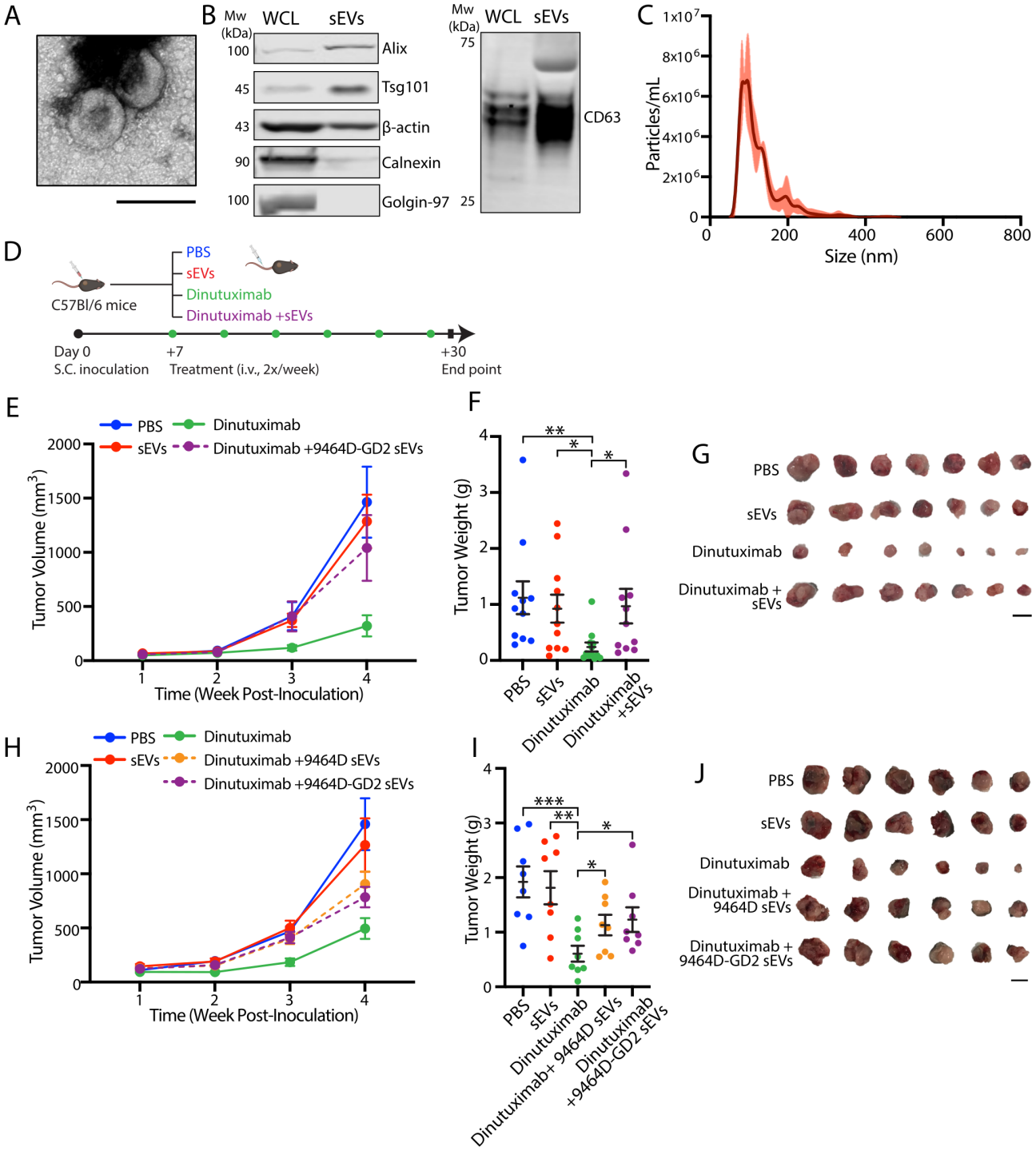

Figure 1 Neuroblastoma-derived sEVs promote resistance to dinutuximab *in vivo*. (A) Representative electron microscopy image of sEVs isolated from 9464D-GD2 cells. Scale bar, 200 nm. (B) Immunoblot of positive and negative sEV markers in WCL and purified sEVs isolated from 9464D-GD2 cells. All lanes loaded with equal amount of protein. (C) Representative size distribution and concentration of sEVs isolated from 9464D-GD2 cells quantified by NTA. Mode 95.3 nm, concentration 4.69×10^8 (D) Experimental design. C57BL/6 mice were subcutaneously inoculated with 1×10^6 9464D-GD2 cells. One-week postinoculation, tumor-bearing mice began receiving tail-vein injections of PBS, dinutuximab (25 µg/mouse) and/or sEVs derived from indicated cell lines (20 µg) two times per week. On day 30, mice were sacrificed and tumors were harvested for analysis. (E) Quantification of tumor volume at indicated time points post-tumor inoculation. Mean±SEM, PBS, n=11; sEVs, n=10; dinutuximab, n=12; dinutuximab+9464D-GD2 sEVs, n=11. Data represent one experiment. (F) Quantification of tumor weight from indicated treatment groups on day 30. Mean±SEM, n as in (E). Two-tailed unpaired t-test. *p<0.05; **p<0.01. (G) Representative images of tumors from treatment groups as in (E) on day 30. Scale bar, 1 cm. (H) Quantification of tumor volume at indicated time points. Mean±SEM, n=8 per group. (I) Tumor weight from indicated treatment groups on day 30. Mean±SEM, n=8 per group. Two-tailed unpaired t-test. *p<0.05; **p<0.01; ***p<0.001. (J) Representative images of tumors from indicated treatment groups on day 30. Scale bar, 1 cm. sEV, small extracellular vesicle; WCL, whole cell lysate.

(figure 1D). As anticipated, dinutuximab dramatically suppressed tumor growth compared with PBS control, highlighting the efficacy of anti-GD2 immunotherapy against 9464D-GD2 tumors *in vivo* (figure 1E). Strikingly, while sEVs alone failed to alter tumor growth compared with control, mice treated with the combination of dinutuximab and sEVs displayed nearly complete resistance to the antitumor effect of dinutuximab (figure 1E). *Ex vivo* quantification of tumor volume and weight at the experimental endpoint confirmed that sEV treatment significantly suppressed the antitumor efficacy of dinutuximab but had no effect on 9464D-GD2 tumor growth when administered alone (figure 1F,G, online supplemental figure S1C).

While the surface expression of GD2 was significantly upregulated in 9464D-GD2 cells, sEVs isolated from these cells showed a moderate increase in GD2 compared with control (online supplemental figure S1D). To investigate whether sEV-associated GD2 promoted resistance to dinutuximab by acting as an antibody decoy to facilitate tumor immune evasion, similar to the immunosuppressive mechanism exhibited by sEV-associated programmed death-ligand 1 (PD-L1), we repeated the *in vivo* experiment and included sEVs derived from both 9464D-GD2 and parental 9464D cell lines (figure 1H).[14] Notably, mice treated with the combination of dinutuximab and either sEVs derived from 9464D parental or 9464D-GD2 cell lines demonstrated a comparable increase in tumor growth compared with mice treated with dinutuximab alone (figure 1H–J, online supplemental figure S1E), suggesting that in this experimental system, sEV-associated GD2 is not the primary factor involved in mediating resistance to anti-GD2 immunotherapy.

Neuroblastoma-derived sEVs suppress dinutuximab-induced NK cell tumor infiltration and enhance the recruitment of tumor-associated macrophages

To elucidate the transcriptome changes underlying sEV-mediated resistance to dinutuximab, we performed RNA sequencing analysis of 9464D-GD2 tumors isolated from mice treated with either dinutuximab or dinutuximab plus sEVs (online supplemental figure S2A–C). Tumors derived from mice treated with the combination of dinutuximab and sEVs demonstrated a significant upregulation in genes involved in myeloid leukocyte-mediated immunity and myeloid cell recruitment, including *Ccr2*,[27] *Clec10a*,[28] and *Clec1a*[29] (online supplemental figure S2D). To further investigate how sEVs mediate changes to the tumor TME, we performed gene set enrichment analysis (GSEA). Intriguingly, pathways involved in myeloid leukocyte-mediated immunity, as well as negative regulation of NK cell-mediated immunity and cytotoxicity, were among the top 20 most significantly enriched pathways in tumors derived from mice treated with dinutuximab plus sEVs (figure 2A, online supplemental tables S2 and S3). Using GSEA of gene sets of interest, we confirmed that sEV treatment induced enrichment of genes involved in myeloid leukocyte-mediated immunity as well as negative regulation of lymphocyte activation (figure 2B,C). In contrast, genes involved in extrinsic apoptotic signaling were less enriched in tumors treated with dinutuximab and sEVs compared with dinutuximab alone (figure 2D).

As the composition of tumor-infiltrating immune cells correlates with sensitivity to immunotherapy, we hypothesized that neuroblastoma-derived sEVs alter the tumor immune microenvironment. To test this hypothesis, we performed flow cytometry to analyze immune cell populations in tumors derived from mice treated with PBS, dinutuximab and/or sEVs (as in figure 1). We were specifically interested in how sEVs affected NK cell tumor infiltration, as patients with tumors that express high levels of the NK cell marker CD56 or NK cell activating receptor NKG2D demonstrate an increased event-free 5-year survival probability compared with patients with low expression of these markers (online supplemental figure S2E,F, see online supplemental table S4 for patient characteristics). We found that treatment with dinutuximab significantly increased the tumor-infiltrating NK cell population compared with control or sEVs alone (figure 2E, see online supplemental figure S3 for gating strategy). Additionally, mice treated with dinutuximab displayed a significant increase in the percentage of serum NK cells compared with control or sEV treatment groups (figure 2F). Strikingly, sEVs significantly suppressed dinutuximab-induced NK cell mobilization and tumor infiltration to a level comparable to control (figure 2E–F).

Myeloid cells also play important roles in regulating neuroblastoma response to immunotherapy, as they create an immunosuppressive TME that suppresses T cell and NK cell proliferation and cytotoxicity.[3] As our RNA sequencing results implicated myeloid cells in sEV-mediated resistance to dinutuximab, we next analyzed tumors for the presence of tumor-associated macrophages (TAMs). Dinutuximab significantly decreased the TAM population compared with all other treatment conditions (figure 2E). Interestingly, tumors derived from mice treated with sEVs alone demonstrated an upregulation in the percentage of TAMs, while those derived from mice treated with the combination of dinutuximab and sEVs demonstrated a percentage of TAMs comparable to control (figure 2E). Collectively, these results suggest that neuroblastoma-derived sEVs induce resistance to dinutuximab by promoting an immunosuppressive TME characterized by a decrease in tumor-infiltrating NK cells and an increase in TAMs.

Neuroblastoma-derived sEVs modulate NK cell maturation in vivo and NK cell-mediated ADCC in vitro

To determine how sEVs promote an immunosuppressive TME, we next asked where they are primarily taken up *in vivo*. We found that Vybrant DiD-labeled sEVs demonstrated significant uptake in the lungs, liver, and spleen within the first 6 hours after tail vein injection (online supplemental figure S4). To determine whether splenic uptake of neuroblastoma-derived sEVs alters

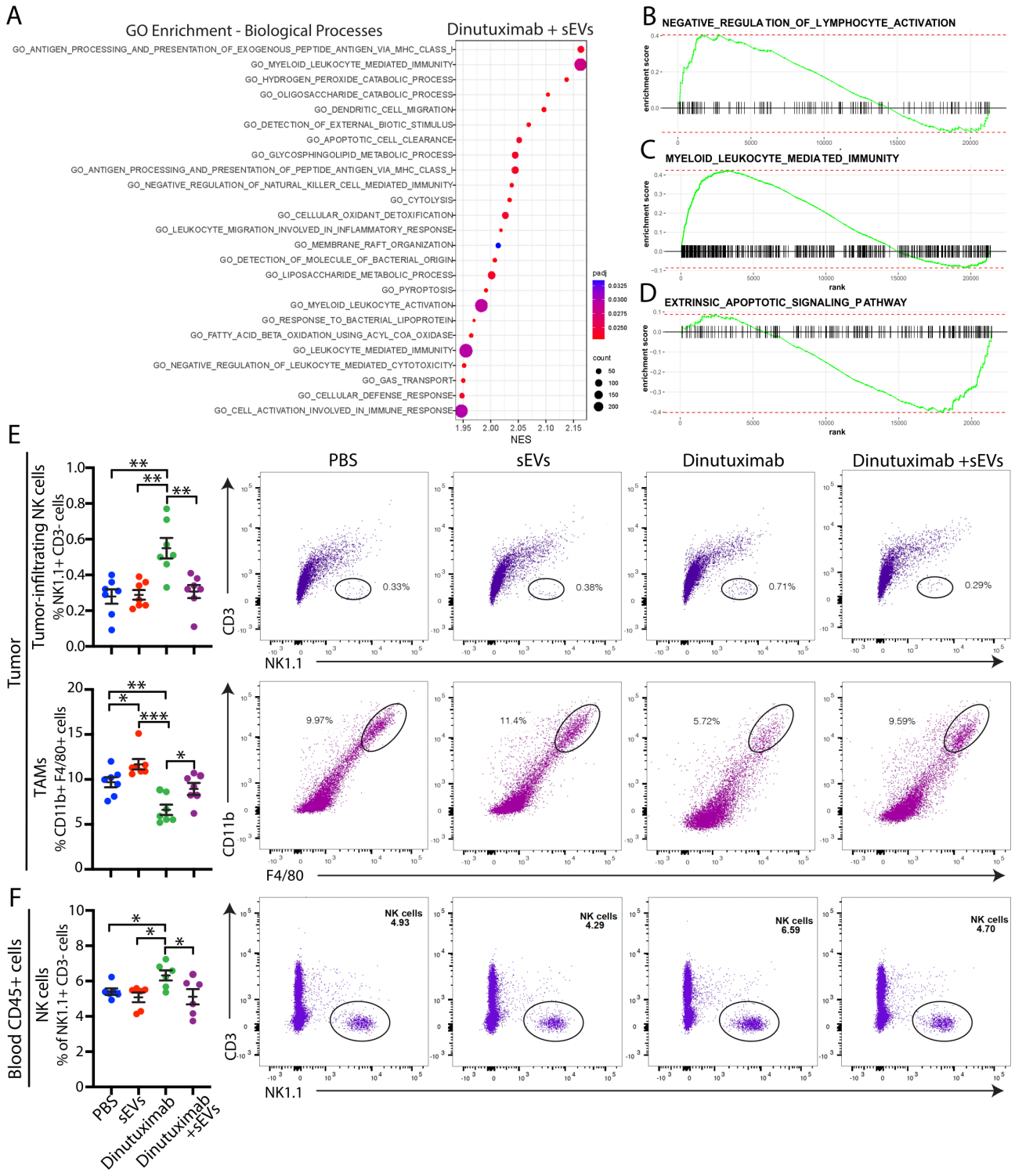

Figure 2 Neuroblastoma-derived sEVs suppress dinutuximab-induced NK cell tumor infiltration and enhance the recruitment of tumor-associated macrophages. (A) Top 20 biological processes identified by GO enrichment analysis of 9464D-GD2 tumors treated with the combination of dinutuximab and sEVs compared with tumors treated with dinutuximab alone, as described in online supplemental figure S2A. (B,C) Select GSEA enrichment plots of clusters enriched in tumors treated with dinutuximab plus sEVs: (B) negative regulation of lymphocyte activation and (C) myeloid leukocyte mediated immunity. (D) GSEA enrichment plot for the extrinsic apoptotic signaling pathway. (E,F) C57BL/6 mice were inoculated with 9464D-GD2 cells and treated as described in figure 1D. (E) Quantification and representative flow cytometry plots of tumor-infiltrating NK cells (NK1.1+CD3-; top panel) and TAMs (CD11b+F4/80+; bottom panel) in 9464D-GD2 tumors isolated from mice in indicated treatment groups on day 30. Mean±SEM, n=7 per group. Student's t-test. *p<0.05; **p<0.01; ***p<0.001. (F) Quantification and representative flow cytometry plots of NK cells (NK1.1+CD3-) isolated from the blood of tumor-bearing mice on day 30 in indicated treatment groups. Mean±SEM, n=7 per group. Student's t-test. *p<0.05; **p<0.01; ***p<0.001. GSEA, gene set enrichment analysis; sEV, small extracellular vesicle; TAM, tumor-associated macrophage.

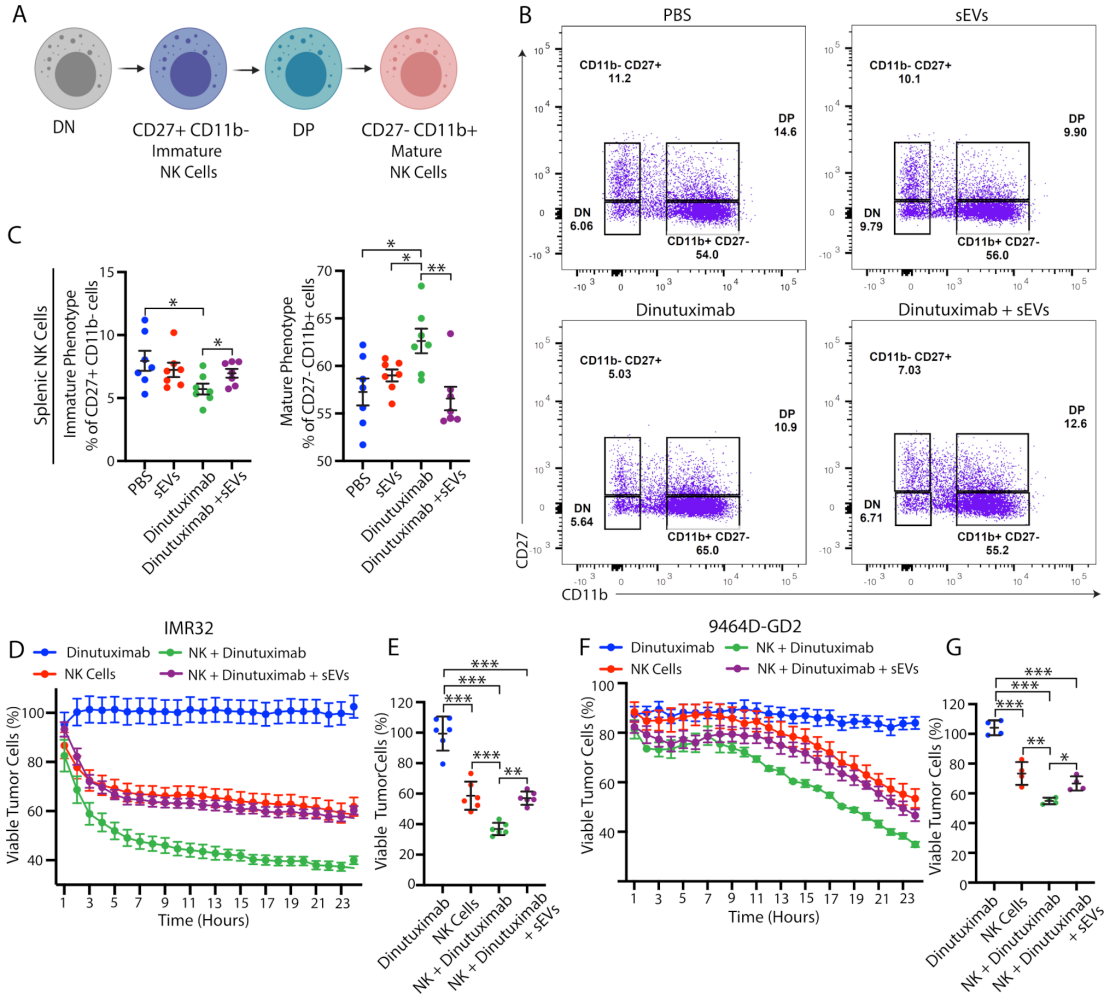

Figure 3 Neuroblastoma-derived sEVs modulate NK cell maturation *in vivo* and NK cell-mediated ADCC *in vitro.* (A) Schematic of NK cell subpopulations. Created with BioRender.com. (B) Representative flow cytometry plots of splenic NK cell subpopulations isolated from 9464D-GD2 tumor-bearing mice receiving the indicated treatments as described in figure 1D. (C) Quantification of the percentage of immature splenic NK cell (CD27 +CD11b- ; left panel) and mature NK cell (CD27- CD11b+; right panel) subpopulations in 9464D-GD2 tumor-bearing mice treated as described in figure 1D. Mean±SEM, n=7 per group. Student's t-test. *p<0.05; **p<0.01; ***p<0.001. (D–G) Human (IMR32) or murine (9464D-GD2) neuroblastoma cells treated as indicated in the presence or absence of NK92-CD16-EGFP cells (NK) and monitored for viability utilizing cell impermeant nucleic acid stain YOYO-3 with the IncuCyte S3 Live-Cell Analysis System. The cell-by-cell analysis module was used to quantify viable tumor cells (YOYO3- EGFP-). (D) Kinetic analysis of the IMR32 in vitro NK-cell-mediated ADCC assay. Mean±SEM, n=6. Viable cells calculated as percentage of viable cells in each treatment condition divided by viable cells in untreated control group. (E) Percentage of viable IMR32 cells at 24 hours, n=6. Mean±SD. One-way ANOVA with Tukey's/Sidak's post hoc tests. **p<0.01; ***p<0.001. (F) Kinetic analysis of the 9464D-GD2 *in vitro* NK-cell-mediated ADCC assay. Mean±SEM, n=4. Viable cells calculated as percentage of viable cells in each treatment condition divided by viable cells in untreated control group. (G) Percentage of viable 9464D-GD2 cells at 24 hours, n=4. Mean±SD. One-way ANOVA with Tukey's/Sidak's post hoc tests. *p<0.05; **p<0.01; ***p<0.001. ADCC, antibody-dependent cell-mediated cytotoxicity; ANOVA, analysis of variance; DN, double negative; DP, double positive; sEV, small extracellular vesicle.

immune cell maturation, we performed flow cytometry analysis on spleens isolated from 9464D-GD2 tumor-bearing mice treated with PBS, dinutuximab and/or sEVs, as in figure 1.[30] Since NK cells are the main immune effector cells that respond to anti-GD2 immunotherapy, we were particularly interested in how sEVs modulate NK cell subpopulations and maturation.[3] We used CD27 and CD11b to subdivide NK cells into four different maturation subsets and focused on both immature CD27+CD11b- cells and mature CD27- CD11b+ cells (figure 3A,B).[31 32] Interestingly, dinutuximab significantly decreased the percentage of immature splenic NK cells and increased the percentage of mature splenic NK cells compared with all other treatment groups, suggesting that dinutuximab promotes NK cell maturation in vivo (figure 3C). Notably, spleens isolated from mice treated with the combination of dinutuximab and sEVs demonstrated NK cell percentages comparable to control levels, suggesting that sEVs suppress dinutuximab-induced NK cell maturation in vivo (figure 3C).

To determine whether neuroblastoma-derived sEVs directly suppress NK cell-mediated ADCC, we next

performed an *in vitro* co-culture experiment using the human NK92 cell line stably expressing CD16 and EGFP (NK92-CD16-EGFP) with either 9464D-GD2 cells or the GD2-positive human neuroblastoma cell line IMR32 (online supplemental figure S5A,B). NK cell-mediated ADCC was monitored in the presence or absence of dinutuximab and sEVs using the cell impermeant nucleic acid stain YOYO-3 and the IncuCyte S3 live-cell analysis system. As expected, the cytotoxic effects of dinutuximab required the presence of NK92-CD16-EGFP immune effector cells, while preincubation of NK92-CD16-EGFP cells with sEVs suppressed dinutuximab-induced NK cell-mediated ADCC against both human and mouse neuroblastoma cell lines (figure 3D–G; online supplemental figure S5C,D). Taken together, these data suggest that sEVs induce resistance to dinutuximab by both modulating NK cell maturation *in vivo* and suppressing NK cell-mediated ADCC.

Inhibition of sEV secretion by tipifarnib suppresses neuroblastoma growth by sensitizing tumors to dinutuximab

After determining that neuroblastoma-derived sEVs induce resistance to anti-GD2 immunotherapy through modulation of the immune system, we next sought to determine whether inhibition of sEV secretion would resensitize tumors to dinutuximab. We first blocked sEV secretion through genetic depletion of *Rab27a*, an essential Rab GTPase involved in sEV secretion.[26] As expected, loss of *Rab27a* in 9464D cells dramatically suppressed sEV secretion *in vitro* (9464D-crRab27a, online supplemental figure S6A,B). However, despite no difference in proliferation *in vitro* compared with parental cells, loss of *Rab27a* dramatically suppressed 9464D tumor growth *in vivo* (online supplemental figure S6C–E), which prevented us from using this genetic model to further dissect the role of sEVs in dinutuximab resistance.

We next sought to use a pharmacologic approach to inhibit sEV secretion through treatment with tipifarnib. Tipifarnib is a potent, selective, and orally bioavailable inhibitor of farnesyltransferase that was recently shown to selectively inhibit sEV secretion from cancer cell lines *in vitro*.[33] As tipifarnib inhibits additional cellular pathways, including RAS signaling, we established that a dose of 0.1 µM significantly suppressed sEV secretion in 9464D-GD2 cells in the absence of cytotoxicity (figure 4A–C, online supplemental figure S7A,B).

To determine whether tipifarnib-mediated inhibition of sEV secretion sensitizes neuroblastoma tumors to dinutuximab *in vivo*, we subcutaneously inoculated C57BL/6 mice with 1×10^6 9464D-GD2 cells. One-week post-inoculation, tumor-bearing mice began receiving two times a week tail-vein injections of PBS or dinutuximab in combination with tipifarnib or an equivalent volume of vehicle by oral gavage two times per day (figure 4D). Mice treated with either tipifarnib or the combination of dinutuximab and tipifarnib demonstrated a significant decrease in circulating sEV concentration compared with mice treated with either vehicle control or dinutuximab alone, as determined by measurement of serum sEV protein and NTA analysis, confirming that tipifarnib suppresses sEV secretion *in vivo* (figure 4E, online supplemental figure S7C,D). Interestingly, mice treated with tipifarnib alone demonstrated a reduction in tumor volume and weight compared with vehicle control, suggesting that tipifarnib suppresses tumor growth *in vivo* through inhibition of sEV secretion and/or other cellular mechanisms (figure 4F–H). Critically, combination treatment with tipifarnib and dinutuximab significantly enhanced the antitumor efficacy of dinutuximab, resulting in a substantial reduction in tumor growth throughout the duration of the experiment compared with single treatment with either agent (figure 4F). At the experimental endpoint, tumors isolated from mice treated with the combination of dinutuximab and tipifarnib demonstrated a significant reduction in weight and volume compared with tumors from mice in all other treatment groups, suggesting that the combination treatment exerts a synergistic antitumor effect (figure 4G,H).

Combination treatment with tipifarnib and dinutuximab suppresses neuroblastoma growth through remodeling of the TME and inhibition of sEV-induced immune suppression

To examine whether tipifarnib sensitizes tumors to dinutuximab by preventing sEV-induced immunosuppression, we analyzed the immune cell composition of 9464D-GD2 tumors and blood isolated from mice treated with vehicle, dinutuximab and/or tipifarnib, as in figure 4D. Consistent with above data, tumors derived from mice treated with dinutuximab demonstrated an immunoreactive TME characterized by enhanced mobilization of NK cells, increased percentages of tumor-infiltrating NK cells and T-cells, and decreased TAMs (figure 5A). Combination treatment with tipifarnib and dinutuximab led to an increase in the percentage of circulating NK cells, as well as the percentage of tumor-infiltrating NK cells and T-cells compared with control or either treatment alone (figure 5A,B), suggesting that tipifarnib and dinutuximab work synergistically to prevent the development of an immunosuppressive TME. Interestingly, while sEV treatment alone upregulated the percentage of TAMs compared with dinutuximab or control (figure 2E), tipifarnib treatment decreased the percentage of TAMs compared with control, and tumors derived from mice treated with the combination of tipifarnib and dinutuximab demonstrated a significant reduction in TAMs compared with all other conditions, suggesting that tumor-derived sEVs promote the recruitment of immunosuppressive macrophages to the TME (figure 5A).

To determine whether tipifarnib prevents sEV-induced systemic immune suppression, we next examined NK cell subsets in the spleen and myeloid cell subpopulations in the BM. We found that both dinutuximab and the combination of dinutuximab and tipifarnib treatment significantly increased the percentage of mature NK cells in the spleen compared with control or tipifarnib alone (figure 5C). Moreover, combination treatment decreased

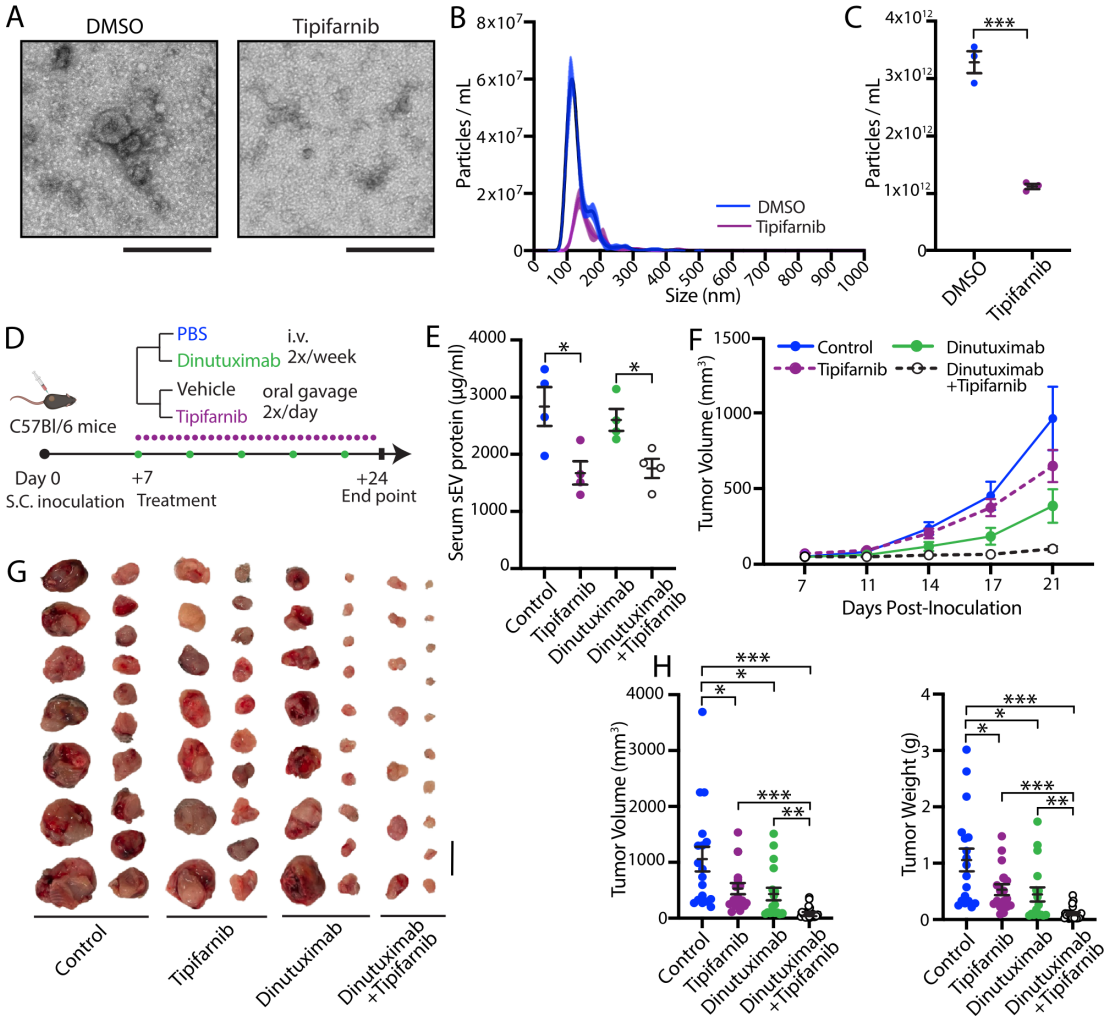

Figure 4 Inhibition of sEV secretion by tipifarnib suppresses neuroblastoma growth by sensitizing 9464D-GD2 tumors to dinutuximab. (A) Representative electron microscopy images of sEVs isolated from 9464D-GD2 cells treated with DMSO or 0.1 µM tipifarnib for 48 hours. Scale bar, 200 nm. (B,C) NTA analysis of sEVs isolated from 9464D-GD2 cells treated with DMSO or 0.1 µM tipifarnib for 48 hours. (B) Representative size distribution and particle concentration. (C) Quantification of particle concentration. Mean±SD, n=4. Student's t-test. ***p<0.001. (D) Experimental design for E–H. C57BL/6 mice were subcutaneously inoculated with 1×10^6 9464D-GD2 cells. One-week post-inoculation, tumor-bearing mice began receiving tail-vein injections of PBS or dinutuximab (25 µg/mouse) two times per week combined with oral administration of vehicle or tipifarnib (25 mg/kg/half day) two times per day. On day 24, mice were sacrificed and tumors were harvested for analysis. (E) Quantification of sEV protein content isolated from serum of mice receiving indicated treatments. Mean±SEM, n=4 per group. Student's t-test. *p<0.05. (F) Quantification of tumor volume at indicated time points. Mean±SEM, n=17 per treatment group. Data represent two independent experiments. (G) Representative images of tumors from indicated treatment groups on day 24. Scale bar, 1 cm. (H) Quantification of tumor volume and weight from indicated treatment groups on day 24. Mean±SEM, n=17 per treatment group. Student's t-test. *p<0.05; **p<0.01; ***p<0.001. Data represent two independent experiments. sEV, small extracellular vesicle.

the percentage of immature splenic NK cells compared with other treatment groups (figure 5C). Recent literature revealed that TAMs are primarily derived from BM rather than splenic progenitor cells[34] and arise from the CD11b+Ly6C^{high} population of circulating mouse monocytes in grafted tumors.[35] As tipifarnib decreased the percentage of TAMs, we next investigated whether treatment also altered immature myeloid cell populations in the BM.[36] Progenitor cells that differentiate toward TAMs are characterized as CD11b+Ly6C^{high}Ly6G^{low}, while cells that differentiate toward tumor-associated neutrophils are CD11b+Ly6C^{low}Ly6G^{high} (figure 5D).[36] Tipifarnib treatment significantly decreased the percentage of CD11b+Ly6C^{high}Ly6G^{low} myeloid cells in the BM and increased the percentage of CD11b+Ly6C^{low}Ly6G^{high} myeloid cells in both the presence and absence of dinutuximab (figure 5E,F, gating strategy in online supplemental figure S3D).

To validate that tipifarnib sensitizes tumors to dinutuximab *in vivo* through inhibition of sEV secretion, we performed a rescue experiment by treating mice with dinutuximab and/or tipifarnib in the presence or absence of neuroblastoma-derived sEVs (figure 6). While both dinutuximab and tipifarnib demonstrated mild antitumor activity alone, the

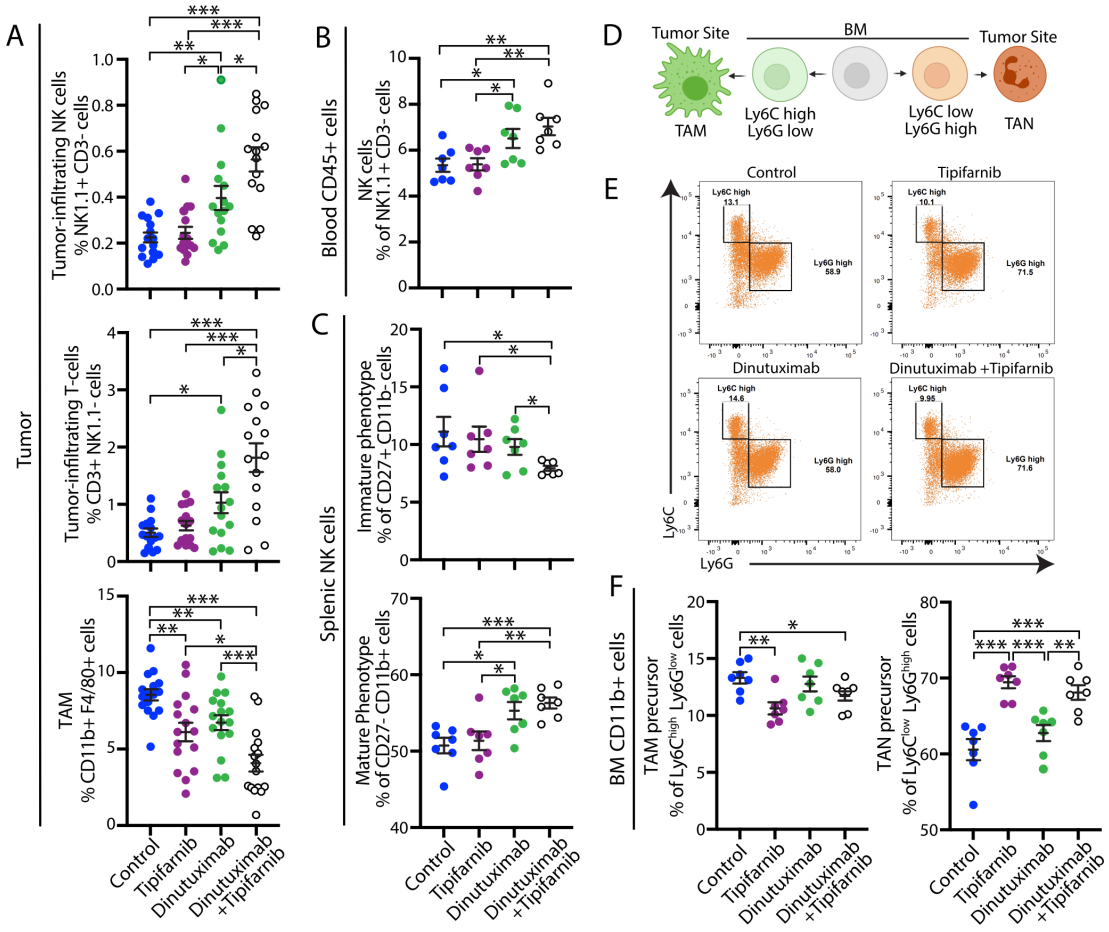

Figure 5 Combination treatment with tipifarnib and dinutuximab suppresses neuroblastoma growth through remodeling of the tumor microenvironment and inhibition of sEV-induced immune suppression. (A) Quantification of tumor-infiltrating NK cells (NK1.1+CD3-; n=15; top panel), tumor-infiltrating T-cells (CD3+NK1.1-; n=15; middle panel) and TAMs (CD11b+F4/80+; n=17; bottom panel) in 9464D-GD2 tumors isolated from mice in the indicated treatment groups on day 24 as described in figure 4D. Mean±SEM. Student's t-test. *p<0.05; **p<0.01; ***p<0.001. Data represent two independent experiments. (B) Quantification of NK cells (NK1.1+/CD3-) isolated from the blood of tumor-bearing mice in the indicated treatment groups on day 24 as described in figure 4D. Mean±SEM, n=7. Student's t-test. *p<0.05; **p<0.01; ***p<0.001. Data represent one experiment. (C) Quantification of the percentage of immature NK cell (CD27+CD11b-; top panel) and mature NK cell (CD27- CD11b+; bottom panel) subpopulations in splenic NK cells isolated from tumor-bearing mice receiving the indicated treatments on day 24 as described in figure 4D. Mean±SEM, n=7. Student's t-test. *p<0.05; **p<0.01; ***p<0.001. (D) Schematic of myeloid cell populations. Image created with BioRender.com. (E) Representative flow cytometry plots of the CD11b+cell subpopulations in BM samples isolated from tumor-bearing mice receiving the indicated treatments as described in figure 4D. (F) Quantification of the percentage of $Ly6C^{high}$ $Ly6G^{low}$ TAM precursor (left panel) and $Ly6C^{low}$ $Ly6G^{high}$ TAN precursor (right panel) subpopulations in BM CD11b+cells isolated from mice on day 24 as described in figure 4D. Mean±SEM, n=7. Student's t-test. *p<0.05; **p<0.01; ***p<0.001. BM, bone marrow; sEV, small extracellular vesicle; TAM, tumor-associated macrophage; TAN, tumor-associated neutrophil.

combination of dinutuximab and tipifarnib significantly decreased tumor growth and weight compared with either agent (figure 6B–D). Notably, the addition of sEVs rescued tumor growth and weight in tipifarnib-treated mice to a level comparable to control, suggesting that inhibition of tumor-derived sEV secretion contributes to the antitumor effects of the drug in vivo (figure 6B–D). Furthermore, sEVs appeared to reverse the antitumor efficacy of dinutuximab plus tipifarnib (figure 6B–D), although the result did not reach statistical significance (p=0.086). Interestingly, we found that the addition of sEVs to combination treatment with dinutuximab and tipifarnib significantly decreased the percentage of tumor-infiltrating NK cells and enhanced the TAM population to a level comparable to dinutuximab treatment alone (figure 6E). Taken together, these results suggest that tipifarnib enhances the efficacy of dinutuximab and modulates the immune system in part through inhibition of sEV secretion.

DISCUSSION

In this study, we demonstrate that neuroblastoma-derived sEVs significantly suppress the efficacy of dinutuximab in vivo and identify the FDA-approved drug tipifarnib as a promising novel adjunct to anti-GD2 immunotherapy, which can be rapidly translated to the clinic for high-risk neuroblastoma patients. Interestingly, our data demonstrate that resistance to dinutuximab is independent of sEV-associated

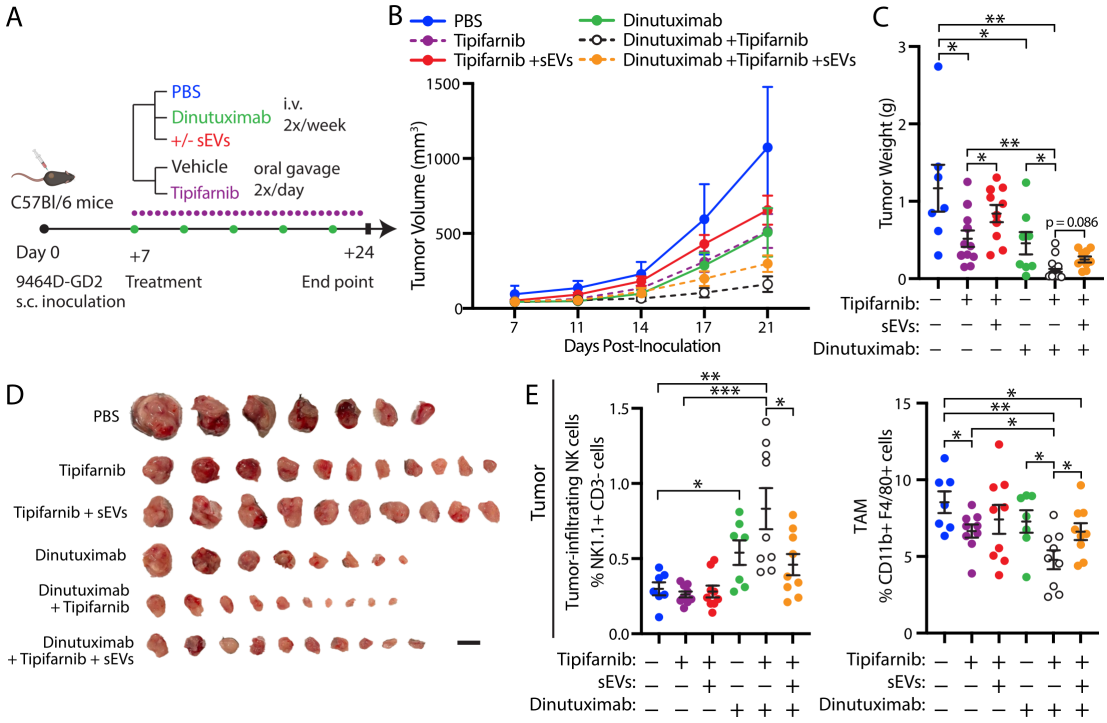

Figure 6 Neuroblastoma-derived sEVs rescue tipifarnib-induced attenuation of tumor growth and reverse the effects of tipifarnib and dinutuximab on tumor immune cell infiltration. (A) Experimental design. C57BL/6 mice were subcutaneously inoculated with 1×10^6 9464D-GD2 cells. One-week postinoculation, tumor-bearing mice began receiving tail-vein injections of PBS control, dinutuximab or dinutuximab plus sEVs two times per week combined with oral administration of vehicle or tipifarnib two times per day. On day 24, tumors were harvested for analysis. (B) Quantification of tumor volume at indicated time points. Mean±SEM. PBS, n=7; tipifarnib, n=11; tipifarnib+sEVs, n=10; dinutuximab, n=8; dinutuximab+tipifarnib, n=10; dinutuximab+tipifarnib+sEVs, n=10. (C) Quantification of tumor weight from indicated treatment groups on day 24. Mean±SEM, n as in (B). Student's t-test. *p<0.05; **p<0.01; ***p<0.001. (D) Representative images of tumors from indicated treatment groups on day 24. Scale bar, 1 cm. (E) Quantification of tumor-infiltrating NK cells (NK1.1+/CD3-; left panel) and tumor-associated macrophages (TAM) (CD11b+/F4/80+; right panel) in 9464D-GD2 tumors isolated from mice in the indicated treatment groups. Mean±SEM, n=7 for PBS and Dinutuximab groups, n=9 for all other groups. Student's t-test. *p<0.05; **p<0.01; ***p<0.001. sEV, small extracellular vesicle.

GD2 expression in this model, suggesting that unlike the well-established mechanism by which sEV-associated PD-L1 interacts with the programmed death-1 receptor on the surface of T cells to suppress their function and promote tumor growth,[14] neuroblastoma-derived sEVs do not serve as a decoy to inhibit the binding of GD2 antibodies and tumor cells. However, this does not preclude the possibility that significant upregulation of sEV-associated GD2 could result in a decoy mechanism to suppress the efficacy of dinutuximab.

Our data reveal that neuroblastoma-derived sEVs modulate immune effector cells both locally and systemically, including NK cells, which are the primary effector cells that mediate dinutuximab-induced killing.[16] Systemically, we found that sEVs suppressed dinutuximab-induced NK cell mobilization and maturation in the spleen. Within the TME, sEVs suppressed dinutuximab-induced NK cell infiltration and upregulated the population of TAMs, promoting an immunosuppressive environment that favored tumor growth. In agreement with our observations, high levels of TAMs are associated with poor outcomes in neuroblastoma patients, while intratumoral NK cells predict improved overall survival.[37 38] Interestingly, we found that tumors isolated from mice treated with both tipifarnib and dinutuximab demonstrated a higher percentage of CD3+ cells, suggesting that T cells may exert an antitumor effect independent of the role of NK cells in this study. These results warrant further investigation, given the well-established function of T cells in neuroblastoma antitumor immunity and the role of sEVs in modulating T cell response.[3 39] Collectively, these data establish that neuroblastoma-derived sEVs modulate the tumor immune cell environment to confer resistance to dinutuximab.

The molecular mechanisms by which neuroblastoma-derived sEVs regulate NK cell function, tumor immune cell recruitment and systemic immune suppression remain unknown. Tumor-derived sEVs have a complex role in modulating the response to immunotherapy.[12 40] sEVs carry an array of immunosuppressive cargo, including miRNA, long non-coding RNA, DNA, and proteins that interfere with the host immune system and reprogram immune effector cells.[12] For example, tumor-derived sEVs inhibit NK cell function through the transfer of miR-23a, leading to CD107a downregulation.[18] Similarly, tumor-derived EVs carry transforming growth factor beta, which inhibits NK cell cytotoxicity by downregulating expression of the activating receptor NKG2.[18 19 41] As sEVs contain a large number of bioactive molecules, we

hypothesize that multiple cargo likely contribute to the immunosuppressive effects of neuroblastoma-derived sEVs, and future studies will be aimed at identifying the critical cargo(s) responsible for resistance to anti-GD2 immunotherapy. In addition, investigation into the molecular mechanisms of sEV biogenesis in neuroblastoma cells will provide additional insight into their immunosuppressive nature and potentially identify other molecules for therapeutic targeting.

The use of the 9464D subcutaneous model offers an immune TME comparable to human neuroblastoma and provides a practical method to test clinically applicable therapies.[42] Future studies into the role of sEVs in anti-GD2 immunotherapy resistance will include the use of orthotopic models, which provide a more representative neuroblastoma TME than subcutaneous tumor models.[43] Interestingly, as dinutuximab targets primary tumor cells less effectively than minimal residual cells in the BM,[10] it is tempting to speculate that the accumulation of tumor-derived sEVs within solid tumors may contribute to local immunosuppression and promote resistance to dinutuximab. Further investigation into the role of circulating and tumor-associated sEVs as well as intratumoral immune cell infiltrates in patients unresponsive to anti-GD2 immunotherapy will provide further insight into the role of sEVs in drug resistance.

Critically, we demonstrated for the first time that tipifarnib, which was recently identified as a selective inhibitor of sEV secretion from cancer cells, significantly enhanced the antitumor efficacy of dinutuximab.[33 44] Mechanistically, tipifarnib inhibits sEV secretion by downregulating several molecules involved in sEV biogenesis and/or secretion, including ALG-2-interacting protein X (Alix), neutral sphingomyelinase 2 and Rab27a.[33 44] Tipifarnib is a potent farnesyltransferase inhibitor that has antitumor activity by inhibiting protumorigenic HRAS signaling.[45] Our data revealed that when given as a single agent tipifarnib exhibited mild antitumor efficacy in neuroblastoma that could be rescued by sEVs, indicating that inhibition of tumor-derived sEV secretion contributes to the antitumor efficacy of tipifarnib in this model. Likewise, neuroblastoma-derived sEVs partially rescued tumor growth and reversed the effects of tipifarnib and dinutuximab on tumor immune cell infiltration. However, we cannot exclude the possibility that systemic administration of tipifarnib inhibited additional farnesylation-dependent pathways that may have contributed to the enhanced antitumor efficacy observed in combination with dinutuximab. Interestingly, alterations in the anaplastic lymphoma kinase-RAS/MAPK pathway correlate strongly with poor clinical outcomes in all neuroblastoma risk categories[46] and are found to be present at a higher frequency in relapsed tumors.[47] Therefore, in addition to inhibiting sEV secretion, administration of tipifarnib with dinutuximab may provide an additional therapeutic benefit to patients harboring aberrant RAS/MAPK signaling pathways. Given that tipifarnib recently entered phase II clinical trials in pediatric patients with advanced solid tumors including neuroblastoma, this combination therapy can be rapidly translated to the clinic to improve outcomes for patients with high-risk neuroblastoma.

Acknowledgements We would like to acknowledge the Department of Comparative Medicine, Bioluminescent Imaging Core, Transmission Electron Microscopy Core, Flow Cytometry Core, and Genome Sciences Core at the Penn State College of Medicine.

Contributors Conceptualization: XL, CAW, H-GW. Data curation: XL, LC, JZ, YZ, MZ. Formal analysis: XL. Validation: XL. Investigation: XL, LC. Visualization: XL. Methodology: XL, CAW, LC, JMS, TS, VSS, H-GW. Writing-original draft: XL, CAW, MMY. Writing-review and editing: XL, MMY, CAW, H-GW. Guarantor: H-GW.

Funding This work was supported in part by the Lois High Berstler Research Endowment Fund and the Four Diamonds Fund of the Penn State College of Medicine.

Competing interests None declared.

Patient consent for publication Not applicable.

Ethics approval All animal studies were performed according to guidelines established by the Institutional Animal Care and Use Committee (IACUC #PRAM201145989) at the Penn State College of Medicine (Hershey, PA).

Provenance and peer review Not commissioned; externally peer reviewed.

Data availability statement Data are available in a public, open access repository. The RNA-sequencing data generated in this study are publicly available in Gene Expression Omnibus (GEO) at GSE189921.

ORCID iD

Carson A Wills http://orcid.org/0000-0003-0356-3071

REFERENCES

1 Irwin MS, Park JR. Neuroblastoma: paradigm for precision medicine. *Pediatr Clin North Am* 2015;62:225–56.
2 Matthay KK, Maris JM, Schleiermacher G, *et al*. Neuroblastoma. *Nat Rev Dis Primers* 2016;2:16078.
3 Wienke J, Dierselhuis MP, Tytgat GAM, *et al*. The immune landscape of neuroblastoma: challenges and opportunities for novel therapeutic strategies in pediatric oncology. *Eur J Cancer* 2021;144:123–50.
4 Casey DL, Cheung N-KV. Immunotherapy of pediatric solid tumors: treatments at a crossroads, with an emphasis on antibodies. *Cancer Immunol Res* 2020;8:161–6.
5 Cheung NK, Saarinen UM, Neely JE, *et al*. Monoclonal antibodies to a glycolipid antigen on human neuroblastoma cells. *Cancer Res* 1985;45:2642–9.
6 Nazha B, Inal C, Owonikoko TK. Disialoganglioside GD2 expression in solid tumors and role as a target for cancer therapy. *Front Oncol* 2020;10:1000.
7 Sait S, Modak S. Anti-GD2 immunotherapy for neuroblastoma. *Expert Rev Anticancer Ther* 2017;17:889–904.
8 Straathof K, Flutter B, Wallace R, *et al*. Antitumor activity without on-target off-tumor toxicity of GD2-chimeric antigen receptor T cells in patients with neuroblastoma. *Sci Transl Med* 2020;12. doi:10.1126/scitranslmed.abd6169. [Epub ahead of print: 25 11 2020].
9 Heczey A, Courtney AN, Montalbano A, *et al*. Anti-GD2 CAR-NKT cells in patients with relapsed or refractory neuroblastoma: an interim analysis. *Nat Med* 2020;26:1686–90.
10 Keyel ME, Reynolds CP. Spotlight on dinutuximab in the treatment of high-risk neuroblastoma: development and place in therapy. *Biologics* 2019;13:1–12.
11 Ahmed M, Cheung N-KV. Engineering anti-GD2 monoclonal antibodies for cancer immunotherapy. *FEBS Lett* 2014;588:288–97.

12 Olejarz W, Dominiak A, Żołnierzak A, *et al*. Tumor-Derived exosomes in immunosuppression and immunotherapy. *J Immunol Res* 2020;2020:1–11.
13 Gao Y, Qin Y, Wan C, *et al*. Small extracellular vesicles: a novel Avenue for cancer management. *Front Oncol* 2021;11:638357.
14 Chen G, Huang AC, Zhang W, *et al*. Exosomal PD-L1 contributes to immunosuppression and is associated with anti-PD-1 response. *Nature* 2018;560:382–6.
15 Poggio M, Hu T, Pai C-C, *et al*. Suppression of exosomal PD-L1 induces systemic anti-tumor immunity and memory. *Cell* 2019;177:e13:414–27.
16 Capuano C, Pighi C, Battella S, *et al*. Harnessing CD16-mediated NK cell functions to enhance therapeutic efficacy of tumor-targeting mAbs. *Cancers* 2021;13. doi:10.3390/cancers13102500. [Epub ahead of print: 20 05 2021].
17 Battke C, Ruiss R, Welsch U, *et al*. Tumour exosomes inhibit binding of tumour-reactive antibodies to tumour cells and reduce ADCC. *Cancer Immunol Immunother* 2011;60:639–48.
18 Berchem G, Noman MZ, Bosseler M, *et al*. Hypoxic tumor-derived microvesicles negatively regulate NK cell function by a mechanism involving TGF-β and miR23a transfer. *Oncoimmunology* 2016;5:e1062968.
19 Zhao J, Schlößer HA, Wang Z, *et al*. Tumor-Derived extracellular vesicles inhibit natural killer cell function in pancreatic cancer. *Cancers* 2019;11. doi:10.3390/cancers11060874. [Epub ahead of print: 22 06 2019].
20 Takahashi Y, Liang X, Hattori T, *et al*. VPS37A directs ESCRT recruitment for phagophore closure. *J Cell Biol* 2019;218:3336–54.
21 Wills CA, Liu X, Chen L, *et al*. Chemotherapy-Induced upregulation of small extracellular vesicle-associated PTX3 accelerates breast cancer metastasis. *Cancer Res* 2021;81:452–63.
22 Barry WE, Jackson JR, Asuelime GE, *et al*. Activated natural killer cells in combination with anti-GD2 antibody Dinutuximab improve survival of mice after surgical resection of primary neuroblastoma. *Clin Cancer Res* 2019;25:325–33.
23 Kroesen M, Brok IC, Reijnen D, *et al*. Intra-adrenal murine TH-MYCN neuroblastoma tumors grow more aggressive and exhibit a distinct tumor microenvironment relative to their subcutaneous equivalents. *Cancer Immunol Immunother* 2015;64:563–72.
24 Kroesen M, Nierkens S, Ansems M, *et al*. A transplantable TH-MYCN transgenic tumor model in C57BL/6 mice for preclinical immunological studies in neuroblastoma. *Int J Cancer* 2014;134:1335–45.
25 Voeller J, Erbe AK, Slowinski J, *et al*. Combined innate and adaptive immunotherapy overcomes resistance of immunologically cold syngeneic murine neuroblastoma to checkpoint inhibition. *J Immunother Cancer* 2019;7:344.
26 Théry C, Witwer KW, Aikawa E, *et al*. Minimal information for studies of extracellular vesicles 2018 (MISEV2018): a position statement of the International Society for extracellular vesicles and update of the MISEV2014 guidelines. *J Extracell Vesicles* 2018;7:1535750.
27 Flores-Toro JA, Luo D, Gopinath A, *et al*. CCR2 inhibition reduces tumor myeloid cells and unmasks a checkpoint inhibitor effect to slow progression of resistant murine gliomas. *Proc Natl Acad Sci U S A* 2020;117:1129–38.
28 Heger L, Balk S, Lühr JJ, *et al*. CLEC10A Is a Specific Marker for Human CD1c^{+} Dendritic Cells and Enhances Their Toll-Like Receptor 7/8-Induced Cytokine Secretion. *Front Immunol* 2018;9:744.
29 Thebault P, Lhermite N, Tilly G, *et al*. The C-type lectin-like receptor CLEC-1, expressed by myeloid cells and endothelial cells, is up-regulated by immunoregulatory mediators and moderates T cell activation. *J Immunol* 2009;183:3099–108.
30 Lewis SM, Williams A, Eisenbarth SC. Structure and function of the immune system in the spleen. *Sci Immunol* 2019;4. doi:10.1126/sciimmunol.aau6085. [Epub ahead of print: 01 03 2019].
31 Chiossone L, Chaix J, Fuseri N, *et al*. Maturation of mouse NK cells is a 4-stage developmental program. *Blood* 2009;113:5488–96.
32 Riggan L, Shah S, O'Sullivan TE. Arrested development: suppression of NK cell function in the tumor microenvironment. *Clin Transl Immunology* 2021;10:e1238.
33 Datta A, Kim H, McGee L, *et al*. High-throughput screening identified selective inhibitors of exosome biogenesis and secretion: a drug repurposing strategy for advanced cancer. *Sci Rep* 2018;8:8161.
34 Shand FHW, Ueha S, Otsuji M, *et al*. Tracking of intertissue migration reveals the origins of tumor-infiltrating monocytes. *Proc Natl Acad Sci U S A* 2014;111:7771–6.
35 Movahedi K, Laoui D, Gysemans C, *et al*. Different tumor microenvironments contain functionally distinct subsets of macrophages derived from Ly6C(high) monocytes. *Cancer Res* 2010;70:5728–39.
36 Bronte V, Brandau S, Chen S-H, *et al*. Recommendations for myeloid-derived suppressor cell nomenclature and characterization standards. *Nat Commun* 2016;7:12150.
37 Melaiu O, Chierici M, Lucarini V, *et al*. Cellular and gene signatures of tumor-infiltrating dendritic cells and natural-killer cells predict prognosis of neuroblastoma. *Nat Commun* 2020;11:5992.
38 Asgharzadeh S, Salo JA, Ji L, *et al*. Clinical significance of tumor-associated inflammatory cells in metastatic neuroblastoma. *J Clin Oncol* 2012;30:3525–32.
39 Ma F, Vayalil J, Lee G, *et al*. Emerging role of tumor-derived extracellular vesicles in T cell suppression and dysfunction in the tumor microenvironment. *J Immunother Cancer* 2021;9:e003217.
40 Li I, Nabet BY. Exosomes in the tumor microenvironment as mediators of cancer therapy resistance. *Mol Cancer* 2019;18:32.
41 Hong C-S, Sharma P, Yerneni SS, *et al*. Circulating exosomes carrying an immunosuppressive cargo interfere with cellular immunotherapy in acute myeloid leukemia. *Sci Rep* 2017;7:14684.
42 Webb ER, Lanati S, Wareham C, *et al*. Immune characterization of pre-clinical murine models of neuroblastoma. *Sci Rep* 2020;10:16695.
43 Grant CN, Wills CA, Liu X, *et al*. Thoracic neuroblastoma: a novel surgical model for the study of extra-adrenal neuroblastoma. *In Vivo* 2022;36:49–56.
44 Zhang H, Lu J, Liu J, *et al*. Advances in the discovery of exosome inhibitors in cancer. *J Enzyme Inhib Med Chem* 2020;35:1322–30.
45 Gilardi M, Wang Z, Proietto M, *et al*. Tipifarnib as a Precision Therapy for *HRAS*-Mutant Head and Neck Squamous Cell Carcinomas. *Mol Cancer Ther* 2020;19:1784–96.
46 Ackermann S, Cartolano M, Hero B, *et al*. A mechanistic classification of clinical phenotypes in neuroblastoma. *Science* 2018;362:1165–70.
47 Eleveld TF, Oldridge DA, Bernard V, *et al*. Relapsed neuroblastomas show frequent RAS-MAPK pathway mutations. *Nat Genet* 2015;47:864–71.

SUPPLEMENTAL MATERIAL

Small extracellular vesicles induce resistance to anti-GD2 immunotherapy unveiling tipifarnib as an adjunct to neuroblastoma immunotherapy

Xiaoming Liu, Carson A. Wills, Longgui Chen, Jiawen Zhang, Yuanjun Zhao, Mi Zhou, Jeffrey M. Sundstrom, Todd D. Schell, Vladimir S. Spiegelman, Megan M. Young and Hong-Gang Wang

Table of Contents

Supplementary Material and Methods

Transduction and CRISPR/Cas9-mediated genome editing

The lentiCas9-Blast (#52962) and LRG (Lenti_sgRNA_EFS_GFP, #65656) plasmids were obtained from Feng Zhang and Christopher Vakoc, respectively, through Addgene. To produce recombinant lentiviruses, each lentiviral vector was co-transfected with the third-generation lentiviral packaging plasmids (pLP1, pLP2, and pLP/VSVG) into HEK 293T/17 cells using jetPRIME transfection reagent (Polyplus, 89129-922). Virus-containing supernatants were collected 24- and 48-hours after transfection, centrifuged (500 RCF) and filtered (0.45-μm pore) prior to storage at -80°C. 9464D cells stably expressing Cas9 were generated by transducing 9464D cells with lentiCas9-Blast followed by selection with blasticidin (40 μg/mL). Cas9expressing 9464D cells were transiently transfected with LRG constructs containing sgRNAs targeting murine Rab27a (5'-TGGTTAAGCTACGAAACCTA-3', 5'AGTGTACTGGTAGAGTACAC-3', 5'-AACCCAGATATAGTGCTGTG-3') followed by FACS sorting to select GFP positive cells 48-hours post-transfection. Single clones were isolated and validated by immunoblotting for Rab27a, and two clones were pooled to establish the Rab27adeficient cell line (9464d crRab27a).

Immunoblotting

Cells were lysed in RIPA lysis buffer containing protease inhibitor cocktail (Sigma-Aldrich, P8340). Whole cell lysate and sEV protein concentrations were determined using a Pierce BCA Protein Assay Kit (VWR Scientific, PI23225) according to manufacturer's instructions. Membranes were blocked in Intercept Blocking Buffer (LI-COR Biosciences,

927-66003) followed by primary antibody incubation at 4˚C overnight. Membranes were washed, incubated with IR-conjugated secondary antibodies for one hour at room temperature (LI-COR Biosciences,

925-32213 and 925-68072) and imaged using the LI-COR Odyssey CLx Imager.

Transmission electron microscopy (TEM)

Microscopy of sEVs was preformed according to a previously described method.[26] Briefly, 10 μL of the sEV sample was loaded onto a 400-mesh copper grid with carbon-coated formvar film and incubated for two minutes. The grid was briefly placed on 10 μL of 2% uranyl acetate for two minutes, followed by blotting to remove excess liquid. The grid was allowed to dry and imaged using a JEOL JEM1400 Transmission Electron Microscope (JEOL USA Inc.).

Nanoparticle tracking analysis (NTA)

sEV samples were diluted to 1 mL (1:1000) with particle-free water. Each sample was loaded by syringe pump into the NanoSight NS300 (Malvern Instruments Ltd) set in scatter mode, and five 60-second videos were generated. The size distribution and concentration of particles were analyzed, and images were acquired using NanoSight software version 3.2 (Malvern Instruments Ltd.). To quantify *in vitro* sEV secretion from neuroblastoma cells upon tipifarnib treatment, cells were treated with DMSO or 0.1 μM tipifarnib in sEV-depleted media for 48 hours. Cells were trypsinized using 0.05% Trypsin-EDTA (VWR Scientific, 45000–660) at the time of conditioned media collection and counted using a Cellometer Auto 2000 Cell Viability Counter (Nexcelom Bioscience). The corresponding sEV pellets were resuspended in 3 μL PBS per 10^6 cells.

Flow cytometric analysis of sEVs

Flow cytometric analysis of sEVs was performed using a protocol adapted from Marimpietr et al.[1] Briefly, 5 μg of purified sEVs was added to 10 μL of 4μm aldehyde/sulfate latex beads (Thermo Fisher, A37304) and incubated for at least 2 hours at room temperature. Twenty μL of 2% FBS in PBS was added to each sample and further incubated for 1 hour at room temperature. The sEVcoated beads were washed with PBS (1 mL) and pelleted at 3,000 RCF for 5 minutes at room temperature. The pellet containing sEV-coated beads was re-suspended in 200 μL of 100 mM glycine in PBS, incubated for 30 minutes at room temperature and pelleted by centrifugation at 3,000 RCF for 5 minutes. The sEV-coated beads were washed twice with 2% FBS in PBS and incubated with FITC-conjugated anti-ganglioside GD2 (BioLegend, clone 14G2a, 1:25 dilution) antibodies in 100 μL FACS buffer for 30 minutes on ice. sEV-coated beads were washed twice with FACS buffer and resuspended in 0.5 mL FACS buffer for flow cytometric analysis.

RNA sequencing and data analysis

Tumors were isolated from mice receiving 5 treatments of dinutuximab or dinutuximab plus sEVs (dosed twice per week as described in the Animal Experiments section). Tumor tissue was flash frozen, and RNA was extracted using RNeasy Mini Kit (Qiagen, 74004). Two RNA samples isolated from female mice tumors in each treatment group were submitted to Penn State College of Medicine Genomic Core Facility for library preparation and sequencing. cDNA libraries weregenerated according to the Illumina Stranded mRNA Prep pipeline(https://www.illumina.com/products/by-type/sequencing-kits/library-prep-kits/stranded-mrnaprep.html). The cDNA library was checked for size distribution using BioAnalyzer

(Agilent). Final libraries were pooled, diluted to 2 nM and subsequently sequenced using the Illumina HiSeq 2500 platform. Adaptors were trimmed from raw FASTQ files using the BBDuk tool. The trimmedFASTQ files were mapped against the mm10 mouse reference genome using STAR aligner (https://physiology.med.cornell.edu/faculty/skrabanek/lab/angsd/lecture_notes/STARmanual.pdf). The aligned reads were quantified with htseq-count (https://htseq.readthedocs.io/en/master/count.html). The differential expression of gene (DEG) analysis was performed using Deseq2 (https://bioconductor.org/packages/release/bioc/html/DESeq2.html) R package. The cutoff is log2FC > 0.5 with an adjusted p-value (FDR) < 0.1. Heatmaps were generated using ComplexHeatmap R package to visualize differential expressed genes. Gene set enrichment analysis was performed using fgsea R package with the Ontology (Biological Process) MSigDB gene set (C5: ontology gene sets, BP: GO Biological Process Ontology).

Kaplan–Meier survival curves

The GSE62564 RNA-Seq dataset containing the gene expression profiles of 498 patient primary neuroblastoma tumors was used for generating Kaplan–Meier survival curve.[2] The Kaplan–Meier event-free survival curve was plotted using survminer R package (https://rpkgs.datanovia.com/survminer/). The total of 498 patient samples were evenly divided into three groups according to the expression level for the desired gene. Red, blue and green lines represent high expression (top 33%), median expression (intermediate 33%) and low expression (bottom 33%) groups.

Tumor and spleen dissociation

Murine tumors and spleens were harvested at the experimental endpoint and mechanically disassociated. Tumors were further digested with tumor digestion buffer (1 mg/mL Collagenase

Type I (Thermo Fisher, 17018029) and 2000 Units/ml DNase (Sigma-Aldrich, DN25-100MG) in HBSS buffer at room temperature for 1 hour. Dissociated tumor cells and spleen cells were passed through a 70 μm cell strainer (Falcon BD, 352350), pelleted, and washed once with PBS supplemented with 1% FBS. Red blood cells were lysed with RBC lysis buffer (0.0155M NH_4Cl, 1.2mM $NaHCO_3$, 0.01mM Na_2EDTA, pH 7.4 in distilled water) for 3 minutes on ice and neutralized with PBS supplemented with 10% FBS. Cells were centrifuged and resuspended in FACS buffer to obtain a single cell suspension.

***In vivo* uptake of neuroblastoma-derived sEVs**

In vivo uptake of neuroblastoma-derived sEVs was performed according to a previously described method.[3] Briefly, sEVs isolated from 9464D-GD2 cells were labeled with 1 mM Vybrant DiD Cell Labeling Solution (Thermo Fisher, V22887) at room temperature for 10 minutes, pelleted by centrifugation at 120,000 RCF for 2 hours at 4°C, and washed once in PBS. Vybrant DiD-labeled pellets were resuspended in PBS and injected (20 μg in 100μL PBS) via the tail vein into C57Bl/6 mice (8- to 10-week-old). At 6-, 12-, and 24-hours after injection, mice were euthanized, whole organs isolated, and fluorescent IVIS imaging was performed. Radiant efficiency was calculated using ROI measurements of each organ.

9464D crRab27a animal experiment

C57Bl/6 mice (8- to 10-week-old, half male and half female) were subcutaneously injected with 1 $x10^6$ 9464D-GD2 cells or 4 $x10^6$ 9464D crRab27a cells in a 50:50 mixture of

DMEM and Matrigel (Corning). After 18 Days, mice were euthanized, and tumors were harvested for analysis.

Cell viability and proliferation assays

9464D-GD2 cells were seeded in a white, opaque 96-well plate. The following day, cells were treated with a dose response of tipifarnib, and cell viability was measured at 24-, 48- and 72-hours post-treatment using the CellTiter-Glo® Luminescent Cell Viability Assay (Promega, G7573) according to manufacturer's instructions. Microplate luminescence was measured using a CLARIOstar (BMG Labtech) plate reader. All data were normalized to non-treated controls. 9464D cells or 9464D crRab27a cells were plated at a density of 5000 cells/well in a 96-well plate and monitored for confluence using the Incucyte S3 Live Cell Imaging System (Sartorius). The percent cell confluence was quantified using Incucyte Basic Cell Analysis package (Sartorius).

sEV isolation from mouse serum

For serum preparation, blood was collected using Microtainer Capillary Blood Collectors (Fisher) and centrifuged for 5 minutes at 500 RCF and 4°C. The supernatant was transferred to a 1.5 mL Eppendorf tube and centrifuged at 2,000 RCF for 15 minutes at 4°C. The supernatant (serum) was collected in a new 1.5 mL Eppendorf tube and stored at -80°C for sEV isolation. For serum sEV isolation, serum samples were thawed on ice and 3-4 samples (equal volume) from each treatment group were pooled (500 μL total volume). The pooled serum sample was centrifuged at 20,000 RCF for 20 minutes at 4°C to remove microvesicles. The supernatant was centrifuged at 120,000 RCF for 4 hours at 4°C to pellet sEVs. The sEV-containing pellet was washed with PBS and centrifuged again at 120,000 RCF for 4 hours at 4°C. sEVs were resuspended in 250 μL PBS and stored at -20°C prior to further analysis. Serum sEV protein

concentration was determined using a Pierce BCA Protein Assay Kit (VWR Scientific PI23225) according to manufacturer's instructions. Serum sEV samples were diluted to 1 mL (1:2000) with particle-free water and quantified by NTA.

Supplementary References

1. Marimpietri D, Petretto A, Raffaghello L, et al. Proteome profiling of neuroblastoma-derived exosomes reveal the expression of proteins potentially involved in tumor progression. PLoS One 2013;8(9):e75054. doi: 10.1371/journal.pone.0075054 [published Online First: 20130919]
2. Su Z, Fang H, Hong H, et al. An investigation of biomarkers derived from legacy microarray data for their utility in the RNA-seq era. Genome Biol 2014;15(12):523. doi: 10.1186/s13059-014-0523-y [published Online First: 20141203]
3. Wills CA, Liu X, Chen L, et al. Chemotherapy-Induced Upregulation of Small Extracellular Vesicle-Associated PTX3 Accelerates Breast Cancer Metastasis. Cancer Res 2021;81(2):452-63. doi: 10.1158/0008-5472.CAN-20-1976 [published Online First: 20201028]

Table S1. Flow cytometry antibody panels.

Panel	Antibody	Clone	Source	Dilution
GD2 expression	FITC anti-human Ganglioside GD2 Antibody #357314	14G2a	BioLegend	1: 25
Tumor infiltrating immune cells	Alexa Fluor® 700 anti-mouse CD45 Antibody #103128	30-F11	BioLegend	1: 250
	PE anti-mouse CD3 Antibody #100206	17A2	BioLegend	1: 100
	Brilliant Violet 421™ anti-mouse NK-1.1 Antibody #108741	PK136	BioLegend	1: 100
	APC anti-mouse/human CD11b Antibody #101212	M1/70	BioLegend	1:100
	FITC anti-mouse F4/80 Antibody #123108	BM8	BioLegend	1: 250
Spleen NK cell subpopulations	PE anti-mouse CD45 Antibody #103106	30-F11	BioLegend	1: 100
	FITC anti-mouse CD3 Antibody #100204	17A2	BioLegend	1: 125

	Brilliant Violet 421™ anti-mouse NK-1.1 Antibody #108741	PK136	BioLegend	1: 100
	APC anti-mouse/human CD11b Antibody #101212	M1/70	BioLegend	1: 100
	APC/Cyanine7 anti-mouse/rat/human CD27 Antibody # 124226	LG.3A10	BioLegend	1: 100
BM myeloid cell subpopulations	PE anti-mouse CD45 Antibody #103106	30-F11	BioLegend	1: 100
	FITC anti-mouse F4/80 Antibody #123108	BM8	BioLegend	1: 250
	APC anti-mouse/human CD11b Antibody #101212	M1/70	BioLegend	1: 100
	Brilliant Violet 421™ anti-mouse Ly-6C Antibody #128032	HK1.4	BioLegend	1: 25
	Alexa Fluor® 700 anti-mouse Ly-6G Antibody #127622	1A8	BioLegend	1: 200
Blood NK cells	PE anti-mouse CD45 Antibody #103106	30-F11	BioLegend	1: 100
	FITC anti-mouse CD3 Antibody #100204	17A2	BioLegend	1: 125
	Brilliant Violet 421™ anti-mouse NK-1.1 Antibody #108741	PK136	BioLegend	1: 100

Table S2. Differentially expressed genes identified by RNA sequencing analysis

Upregulated and downregulated genes identified in tumors derived from mice treated with dinutuximab and sEVs compared to tumors derived from mice treated with dinutuximab alone, padj < 0.1 & log2FC > 0.5.

Down regulated genes in Dinutuximab&sEVs treated tumors							
Ensembl ID	baseMean	log2FoldChange	lfcSE	stat	pvalue	padj	Gene symbol
ENSMUSG00000028645	10405.9757	-0.9813139	0.1577135	-6.2221298	4.90E-10	6.03E-06	Slc2a1
ENSMUSG00000029752	2374.94142	-1.0452273	0.17785305	-5.8769152	4.18E-09	1.71E-05	Asns
ENSMUSG00000029135	1715.42465	-0.975541	0.17172698	-5.680767	1.34E-08	3.30E-05	Fosl2
ENSMUSG00000035783	312.699733	-2.0479863	0.36570568	-5.6000944	2.14E-08	4.39E-05	Acta2
ENSMUSG00000000628	2115.94534	-0.9791543	0.17617698	-5.5577879	2.73E-08	4.80E-05	Hk2
ENSMUSG00000001493	229.100988	-1.680422	0.31371762	-5.3564793	8.49E-08	0.00013037	Meox1
ENSMUSG00000007872	860.25656	-1.020318	0.20056003	-5.0873449	3.63E-07	0.00049585	Id3
ENSMUSG00000028364	178.805124	-1.8618141	0.39057599	-4.7668422	1.87E-06	0.00194061	Tnc
ENSMUSG00000019997	141.908149	-1.7635547	0.3835121	-4.5984331	4.26E-06	0.00342421	Ccn2
ENSMUSG00000038418	577.131732	-0.985648	0.21286052	-4.6304875	3.65E-06	0.00342421	Egr1
ENSMUSG00000010760	1190.55384	-0.9265077	0.2013865	-4.6006446	4.21E-06	0.00342421	Phlda2
ENSMUSG00000032715	500.589297	-0.9465518	0.20808065	-4.548966	5.39E-06	0.00384373	Trib3
ENSMUSG00000028339	323.632621	-1.1700294	0.25982717	-4.5031064	6.70E-06	0.00411514	Col15a1
ENSMUSG00000005667	1500.57813	-0.9286606	0.20873204	-4.4490562	8.62E-06	0.00504759	Mthfd2
ENSMUSG00000026628	364.149393	-1.107418	0.25036328	-4.4232446	9.72E-06	0.0054316	Atf3
ENSMUSG00000031375	4157.58688	-0.8493333	0.19281469	-4.4049203	1.06E-05	0.00547588	Bgn

ENSMUSG00000008136	684.405384	-0.8525792	0.1950499	-4.3710826	1.24E-05	0.00607775	Fhl2
ENSMUSG00000030103	2805.7872	-0.7096519	0.16606923	-4.2732291	1.93E-05	0.009107	Bhlhe40
ENSMUSG00000004891	135.307765	-1.4780497	0.35070729	-4.2144822	2.50E-05	0.01098866	Nes
ENSMUSG00000025025	3570.7624	-0.6482644	0.15689006	-4.1319659	3.60E-05	0.01524273	Mxi1
ENSMUSG00000032085	101.83896	-2.0933086	0.51575931	-4.0586928	4.93E-05	0.01895279	Tagln
ENSMUSG00000042115	187.694342	-1.2890199	0.32579418	-3.9565468	7.60E-05	0.02748659	Klhdc8a
ENSMUSG00000029661	218.785285	-1.5762	0.40048704	-3.935708	8.30E-05	0.02912793	Col1a2
ENSMUSG00000032135	631.610755	-0.867714	0.22304405	-3.8903259	0.00010011	0.03417634	Mcam
ENSMUSG00000043421	1845.83878	-0.8646789	0.22348049	-3.8691471	0.00010922	0.03627767	Hilpda
ENSMUSG00000039114	2713.49418	-0.6043841	0.1568332	-3.8536743	0.00011636	0.0374817	Nrn1
ENSMUSG00000046727	981.083909	-0.7690106	0.20096449	-3.8265995	0.00012993	0.03991966	Cystm1
ENSMUSG00000031465	474.12095	-0.8871814	0.23651953	-3.750986	0.00017614	0.04884619	Angpt2
ENSMUSG00000058881	1139.86983	-0.7015208	0.18698194	-3.7518105	0.00017556	0.04884619	Zfp516
ENSMUSG00000035969	896.436588	-0.7894875	0.21248404	-3.7155145	0.00020279	0.05352637	Rusc2
ENSMUSG00000056481	137.445075	-1.3053118	0.3525765	-3.7022087	0.00021373	0.05360716	Cd248
ENSMUSG00000029378	763.052247	-0.8382169	0.22638192	-3.702667	0.00021335	0.05360716	Areg
ENSMUSG00000037705	271.96229	-1.0047581	0.27411701	-3.6654351	0.00024692	0.05517504	Tecta
ENSMUSG00000031502	4143.25847	-0.6645208	0.18115049	-3.6683358	0.00024413	0.05517504	Col4a1
ENSMUSG00000010755	2627.03609	-0.6623743	0.18043365	-3.6710133	0.00024159	0.05517504	Cars
ENSMUSG00000024640	7192.68456	-0.5220923	0.14277862	-3.6566561	0.00025553	0.056079	Psat1
ENSMUSG00000073700	1618.3847	-0.7198303	0.19729902	-3.6484232	0.00026386	0.05689079	Klhl21
ENSMUSG00000064337	22159.5274	-0.5223783	0.14410328	-3.6250271	0.00028893	0.06122352	mt-Rnr1
ENSMUSG00000050914	1320.76126	-0.9135222	0.25455556	-3.5886947	0.00033234	0.06922765	Ankrd37
ENSMUSG00000021831	6378.1338	-0.7372291	0.20598342	-3.5790699	0.00034482	0.07063046	Ero1a
ENSMUSG00000037010	448.092528	-1.0266666	0.28722617	-3.5744187	0.00035101	0.07071926	Apln
ENSMUSG00000027313	57.2686016	-1.8930341	0.53238617	-3.5557537	0.0003769	0.07457921	Chac1
ENSMUSG00000032589	927.628515	-0.6445861	0.18147086	-3.5520089	0.0003823	0.07457921	Bsn
ENSMUSG00000035105	4028.13338	-0.7384505	0.20879354	-3.5367499	0.00040508	0.07659186	Egln3
ENSMUSG00000038552	554.804561	-0.7966995	0.22636731	-3.519499	0.00043236	0.0782356	Fndc4
ENSMUSG00000021754	484.066295	-0.7503309	0.21390868	-3.507716	0.00045197	0.0782356	Map3k1
ENSMUSG00000030268	3785.18945	-0.7211888	0.20547457	-3.509869	0.00044833	0.0782356	Bcat1
ENSMUSG00000005125	8368.80762	-0.6138782	0.17460228	-3.5158657	0.00043832	0.0782356	Ndrg1
ENSMUSG00000028072	96.0349014	-1.434501	0.40997726	-3.498977	0.00046705	0.07972229	Ntrk1
ENSMUSG00000015090	108.871164	-1.3332852	0.38275833	-3.4833605	0.00049516	0.08254946	Ptgds
ENSMUSG00000047604	156.55662	-1.1184939	0.32216613	-3.4717923	0.000517	0.08254946	Frat2
ENSMUSG00000060639	524.178589	-0.7302466	0.21034327	-3.4716898	0.00051719	0.08254946	H4c9
ENSMUSG00000020186	1938.19162	-0.6300322	0.18144219	-3.4723579	0.00051591	0.08254946	Csrp2
ENSMUSG00000020593	461.650071	-0.7493051	0.21863814	-3.427147	0.00060996	0.09370491	Lpin1
ENSMUSG00000042622	1055.47436	-0.7463967	0.21803571	-3.4232775	0.00061871	0.0938757	Maff
ENSMUSG00000046432	2322.02821	-0.7231929	0.21351872	-3.3870236	0.00070655	0.09867655	Bex3
ENSMUSG00000037580	1478.31245	-0.7172581	0.2120177	-3.3830106	0.00071696	0.09900476	Gch1
Up regulated genes in Dinutuximab&sEVs treated tumors							
Ensembl ID	baseMean	log2FoldChange	lfcSE	stat	pvalue	padj	Gene symbol
ENSMUSG00000016194	107.6668914	2.565707159	0.430940973	5.953732229	2.62E-09	1.61E-05	Hsd11b1
ENSMUSG00000016024	592.6154412	1.318482216	0.230159779	5.72855179	1.01E-08	3.11E-05	Lbp
ENSMUSG00000024691	1730.348259	0.805657345	0.159725498	5.044012098	4.56E-07	0.000560265	Fam111a
ENSMUSG00000000318	584.7081328	1.025410807	0.215226629	4.764330566	1.89E-06	0.001940608	Clec10a
ENSMUSG00000026034	1307.338702	0.845992567	0.184360062	4.58880604	4.46E-06	0.003424212	Clk1
ENSMUSG00000021903	1139.018806	0.953810719	0.21122479	4.515619209	6.31E-06	0.004083645	Galnt15
ENSMUSG00000090210	883.816782	0.982402767	0.223138624	4.402656734	1.07E-05	0.005475875	Itga10

ENSMUSG00000033082	899.6470668	0.973647247	0.230768731	4.219147204	2.45E-05	0.01098866	Clec1a
ENSMUSG00000039883	478.8842613	1.05961522	0.260183768	4.072564661	4.65E-05	0.01843432	Lrrc17
ENSMUSG00000039476	162.22944	1.345994115	0.338602369	3.975146776	7.03E-05	0.026194781	Prrx2
ENSMUSG00000040950	1341.348646	0.645193199	0.167656749	3.848298395	0.000118941	0.037481702	Mgl2
ENSMUSG00000060600	960.3440305	1.036560425	0.271668553	3.815533353	0.000135889	0.040733586	Eno3
ENSMUSG00000020689	3096.839678	0.590807441	0.156637036	3.77182471	0.000162058	0.047421284	Itgb3
ENSMUSG00000096965	310.1665262	1.353521983	0.361213157	3.747155815	0.000178851	0.048846194	3300005D01Rik
ENSMUSG00000001864	1284.476943	0.795443225	0.214223478	3.713146816	0.000204698	0.053526365	Aif1l
ENSMUSG00000062421	5678.68971	0.61177017	0.165923182	3.6870687	0.000226852	0.055175039	Arf2
ENSMUSG00000038860	607.6332108	0.963433263	0.261868065	3.679078858	0.000234078	0.055175039	Garnl3
ENSMUSG00000022887	108.2045277	1.485809085	0.404284591	3.675156359	0.000237704	0.055175039	Masp1
ENSMUSG00000073557	777.896025	0.663898856	0.187647998	3.538001275	0.000403168	0.076591862	Ppp1r12b
ENSMUSG00000022324	1769.090135	0.585504806	0.166750104	3.511271017	0.000445969	0.078235604	Matn2
ENSMUSG00000049858	372.7654069	1.249103286	0.354852645	3.520061931	0.000431446	0.078235604	Suox
ENSMUSG00000032679	262.1887243	1.039711104	0.299250999	3.47437805	0.000512039	0.082549462	Cd59a
ENSMUSG00000049103	267.9107725	1.119405115	0.323288816	3.462554409	0.000535074	0.08430841	Ccr2
ENSMUSG00000016494	1312.781231	0.62136512	0.180396125	3.444448271	0.000572226	0.089021	Cd34
ENSMUSG00000034714	1416.332881	0.60725538	0.178297263	3.405859242	0.000659562	0.096661457	Ttyh2
ENSMUSG00000017144	1026.505295	0.624415774	0.183534534	3.402170484	0.000668529	0.096661457	Rnd3
ENSMUSG00000052305	740.4675223	0.932987965	0.274211634	3.402437569	0.000667876	0.096661457	Hbb-bs
ENSMUSG00000032271	289.2659113	0.868349205	0.255879771	3.393582864	0.000689847	0.097804531	Nnmt

Table S3. Gene set enrichment analysis (GSEA)

Top 60 up regulated GOBP pathways identified in tumors derived from mice treated with the combination of dinutuximab and sEVs compared to dinutuximab alone.

GOBP pathway	pval	padj	ES	NES
GO_ANTIGEN_PROCESSING_AND_PRESENTATION_OF_EXOGENOUS_PEPTIDE_ANTIGEN_VIA_MHC_CLASS_I	0.00231	0.02388	0.53118	2.16290
GO_MYELOID_LEUKOCYTE_MEDIATED_IMMUNITY	0.00294	0.02796	0.42395	2.16236
GO_PRIMARY_ALCOHOL_METABOLIC_PROCESS	0.00226	0.02363	0.53595	2.16118
GO_HYDROGEN_PEROXIDE_CATABOLIC_PROCESS	0.00216	0.02309	0.65574	2.13702
GO_OLIGOSACCHARIDE_CATABOLIC_PROCESS	0.00213	0.02292	0.88775	2.10372
GO_DENDRITIC_CELL_MIGRATION	0.00217	0.02310	0.65304	2.09657
GO_DETECTION_OF_EXTERNAL_BIOTIC_STIMULUS	0.00221	0.02324	0.69185	2.06825
GO_APOPTOTIC_CELL_CLEARANCE	0.00228	0.02383	0.56331	2.05149
GO_GLYCOSPHINGOLIPID_METABOLIC_PROCESS	0.00233	0.02388	0.53581	2.04447
GO_ANTIGEN_PROCESSING_AND_PRESENTATION_OF_PEPTIDE_ANTIGEN_VIA_MHC_CLASS_I	0.00231	0.02388	0.48711	2.04434
GO_NEGATIVE_REGULATION_OF_NATURAL_KILLER_CELL_MEDIATED_IMMUNITY	0.00215	0.02305	0.78490	2.03787
GO_CYTOLYSIS	0.00218	0.02310	0.65150	2.03424
GO_CELLULAR_OXIDANT_DETOXIFICATION	0.00231	0.02388	0.48499	2.02597
GO_PRIMARY_ALCOHOL_CATABOLIC_PROCESS	0.00424	0.03249	0.76651	2.02249
GO_LEUKOCYTE_MIGRATION_INVOLVED_IN_INFLAMMATORY_RESPONSE	0.00216	0.02309	0.75629	2.01870
GO_MEMBRANE_RAFT_ORGANIZATION	0.00442	0.03348	0.63997	2.01362
GO_DETECTION_OF_MOLECULE_OF_BACTERIAL_ORIGIN	0.00215	0.02305	0.77316	2.00738
GO_LIPOSACCHARIDE_METABOLIC_PROCESS	0.00233	0.02389	0.46799	2.00126
GO_PYROPTOSIS	0.00213	0.02292	0.86457	1.99163
GO_MYELOID_LEUKOCYTE_ACTIVATION	0.00316	0.02903	0.38424	1.98290
GO_RESPONSE_TO_BACTERIAL_LIPOPROTEIN	0.00213	0.02292	0.85507	1.96974
GO_FATTY_ACID_BETA_OXIDATION_USING_ACYL_COA_OXIDASE	0.00219	0.02310	0.71701	1.96398
GO_LEUKOCYTE_MEDIATED_IMMUNITY	0.00324	0.02944	0.37145	1.95498
GO_NEGATIVE_REGULATION_OF_LEUKOCYTE_MEDIATED_CYTOTOXICITY	0.00219	0.02310	0.71260	1.95191
GO_GAS_TRANSPORT	0.00219	0.02310	0.71201	1.95030
GO_CELLULAR_DEFENSE_RESPONSE	0.00228	0.02383	0.53471	1.94734
GO_CELL_ACTIVATION_INVOLVED_IN_IMMUNE_RESPONSE	0.00326	0.02956	0.37549	1.94667
GO_OXYGEN_TRANSPORT	0.00210	0.02268	0.76099	1.94311
GO_LEUKOCYTE_MEDIATED_CYTOTOXICITY	0.00233	0.02388	0.46793	1.93697
GO_DENDRITIC_CELL_CHEMOTAXIS	0.00442	0.03348	0.64360	1.92403
GO_POSITIVE_REGULATION_OF_TOLL_LIKE_RECEPTOR_SIGNALING_PATHWAY	0.00442	0.03348	0.61045	1.92073
GO_REGULATION_OF_T_CELL_CHEMOTAXIS	0.00219	0.02310	0.70118	1.92063
GO_SYNAPSE_PRUNING	0.00217	0.02310	0.78295	1.92048
GO_NEGATIVE_REGULATION_OF_INTERLEUKIN_2_PRODUCTION	0.00445	0.03367	0.63413	1.91824
GO_GANGLIOSIDE_BIOSYNTHETIC_PROCESS	0.00430	0.03291	0.73783	1.91566
GO_PHAGOCYTOSIS	0.00271	0.02626	0.39971	1.90680

GO_EXOCYTOSIS	0.00347	0.02968	0.36123	1.90641
GO_RESPONSE_TO_XENOBIOTIC_STIMULUS	0.00230	0.02388	0.44919	1.90410
GO_LEUKOCYTE_CHEMOTAXIS_INVOLVED_IN_INFLAMMATORY_RESPONSE	0.00204	0.02214	0.89636	1.90156
GO_COMPLEMENT_ACTIVATION_ALTERNATIVE_PATHWAY	0.00217	0.02310	0.77291	1.89583
GO_MEMBRANE_LIPID_CATABOLIC_PROCESS	0.00220	0.02317	0.56616	1.89476
GO_GANGLIOSIDE_METABOLIC_PROCESS	0.00438	0.03335	0.63937	1.89445
GO_DETOXIFICATION	0.00237	0.02394	0.43438	1.89052
GO_NATURAL_KILLER_CELL_MEDIATED_IMMUNITY	0.00462	0.03447	0.49398	1.88078
GO_REGULATION_OF_NATURAL_KILLER_CELL_MEDIATED_IMMUNITY	0.00231	0.02388	0.54205	1.87946
GO_FLAVONOID_METABOLIC_PROCESS	0.00640	0.04318	0.81294	1.87269
GO_POSITIVE_REGULATION_OF_PHAGOCYTOSIS	0.00235	0.02391	0.48056	1.87144
GO_NEGATIVE_REGULATION_OF_CELL_KILLING	0.00452	0.03408	0.64531	1.86938
GO_COMPLEMENT_ACTIVATION	0.00234	0.02389	0.47399	1.86906
GO_IMMUNE_EFFECTOR_PROCESS	0.00400	0.03124	0.34829	1.86381
GO_IMMUNE_RESPONSE_INHIBITING_SIGNAL_TRANSDUCTION	0.00415	0.03195	0.83735	1.85429
GO_MEMBRANE_LIPID_METABOLIC_PROCESS	0.00243	0.02398	0.39814	1.85067
GO_HYDROGEN_PEROXIDE_METABOLIC_PROCESS	0.00232	0.02388	0.49819	1.85030
GO_MONOACYLGLYCEROL_BIOSYNTHETIC_PROCESS	0.00204	0.02214	0.86988	1.84539
GO_CELLULAR_RESPONSE_TO_TOXIC_SUBSTANCE	0.00237	0.02394	0.42871	1.84094
GO_POSITIVE_REGULATION_OF_T_CELL_MIGRATION	0.00438	0.03335	0.55518	1.82789
GO_CELLULAR_LIPID_CATABOLIC_PROCESS	0.00256	0.02504	0.39250	1.82681
GO_REGULATION_OF_PHAGOCYTOSIS	0.00229	0.02388	0.43891	1.82342
GO_REGULATION_OF_T_CELL_MIGRATION	0.00229	0.02385	0.51151	1.81675
GO_NLS_BEARING_PROTEIN_IMPORT_INTO_NUCLEUS	0.00656	0.04408	0.61311	1.81664

Table S4. GSE62564 Patient Characteristics

GSE62564 Patient Characteristics	
Total Patients	498
Gender	
Male	287
Female	211
Risk stratification	
High risk	176
Low/unknown risk	322
Age at diagnosis (years)	
0-1	212
1-5	243
5-10	32
10-15	8
>15	3
Overall survival (years)	
0-1	32
1-5y	197
5-10	191
10-15	73
>15	5
Event-free survival (years)	
0-1	95
1-5	183
5-10	151
10-15	66
>15	3

Figure S1

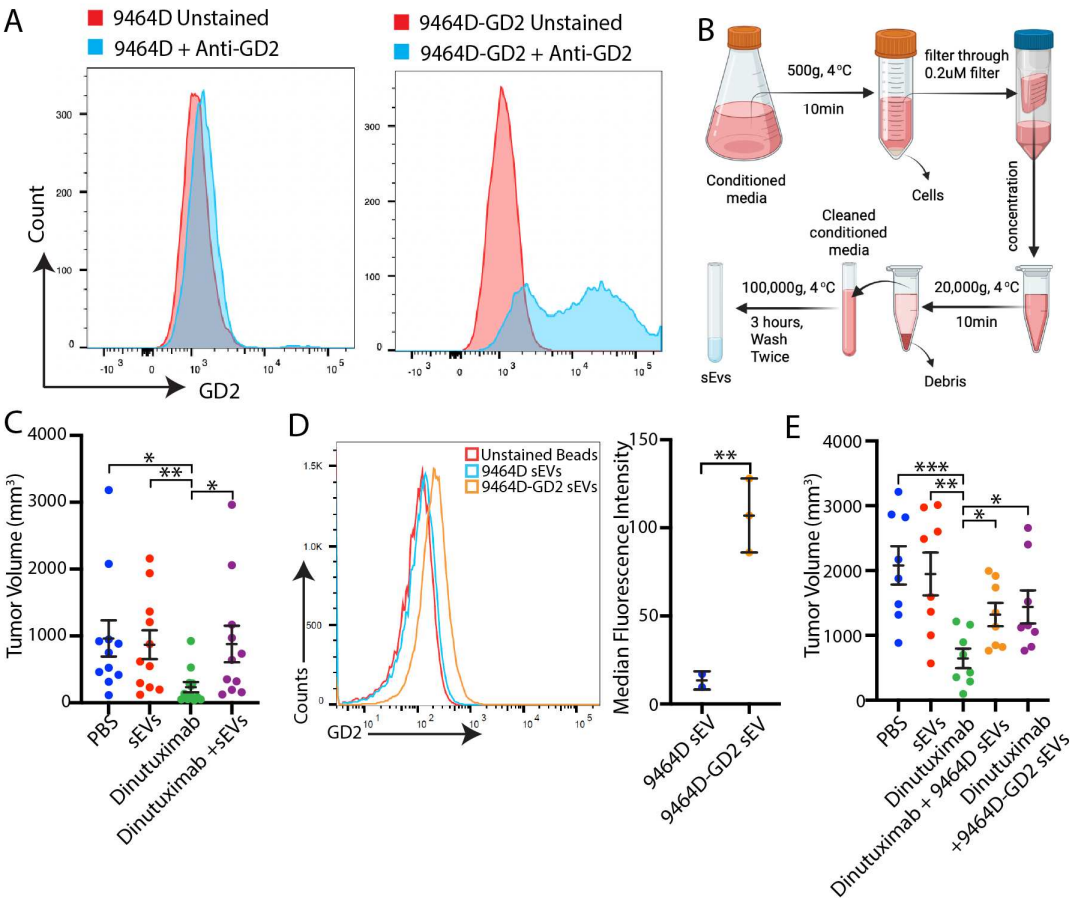

Figure S1. Overexpression of GM2/GD2 synthase and GD3 synthase upregulate cell surface expression of GD2 and sensitize 9464D-GD2 tumors to dinutuximab.
(A) Flow cytometry analysis of cell surface expression level of GD2 in 9464D cells and 9464D-GD2 cells. (B) Schematic of sEV isolation from cell culture by differential ultracentrifugation. Created with BioRender.com (C) Quantification of tumor volume from indicated treatment groups on day 30, as in Figure 1E. Mean ± SEM, PBS, n = 11; sEVs, n = 10; dinutuximab, n = 12; dinutuximab +sEVs, n = 11. Two-tailed unpaired t-test. *, $p < 0.05$; **, $p < 0.01$. (D) Flow cytometry analysis detecting the presence of GD2 on the surface of sEVs derived from 9464D cells and 9464D-GD2 cells absorbed onto latex beads (left). Median fluorescence intensity of GD2 corrected by unstained beads (right). Mean ± SD, 9464D sEV, n=2; 9464D-GD2 sEV, n=3. Two-tailed unpaired t-test. **, $p < 0.01$. (E) Quantification of tumor volume from indicated treatment groups on day 30, as in figure 1H. Mean ± SEM, n = 8 per group. Two-tailed unpaired t-test. *, $p < 0.05$; **, $p < 0.01$; ***, $p < 0.001$.

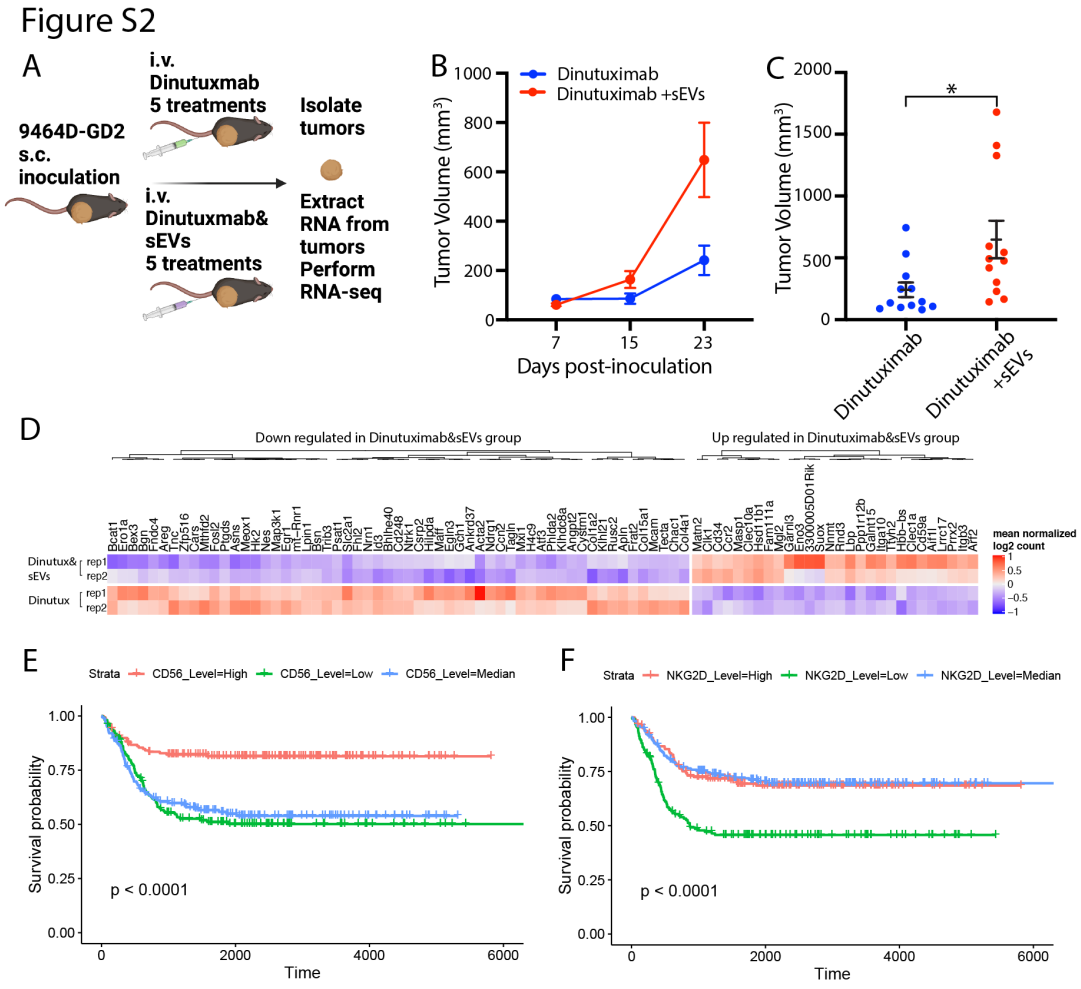

Figure S2. sEVs modulate the transcriptome of immunoregulatory genes in 9464D-GD2 tumors while neuroblastoma patients with high expression of NK cell markers display a survival advantage.

(A) Experimental design for B-D and Figure 2A-D (created with BioRender.com). C57Bl/6 mice were subcutaneously inoculated with 1 x10^6 9464D-GD2 cells. One-week post-inoculation, tumor-bearing mice began receiving tail-vein injections with dinutuximab (25 µg/mouse) or the combination of dinutuximab (25 µg/mouse) and sEVs (20 µg) twice per week. On day 23, tumors were harvested for RNA-sequencing analysis. (B) Quantification of tumor volume at indicated time points. Mean ± SEM, n = 12 per treatment group. (C) Quantification of tumor volume from indicated treatment groups on day 23. Mean ± SEM, n = 12 per treatment group. Two-tailed unpaired t-test. *, $p < 0.05$. (D) Heatmap of differentially expressed genes for tumors treated with dinutuximab plus sEVs compared to dinutuximab alone. Vst transformed reads over row mean normalization. (E) Kaplan-Meier Curve of event-free survival according to CD56 expression. (F) KaplanMeier Curve of event-free survival according to NKG2D expression. Data obtained from the GSE62564 dataset.

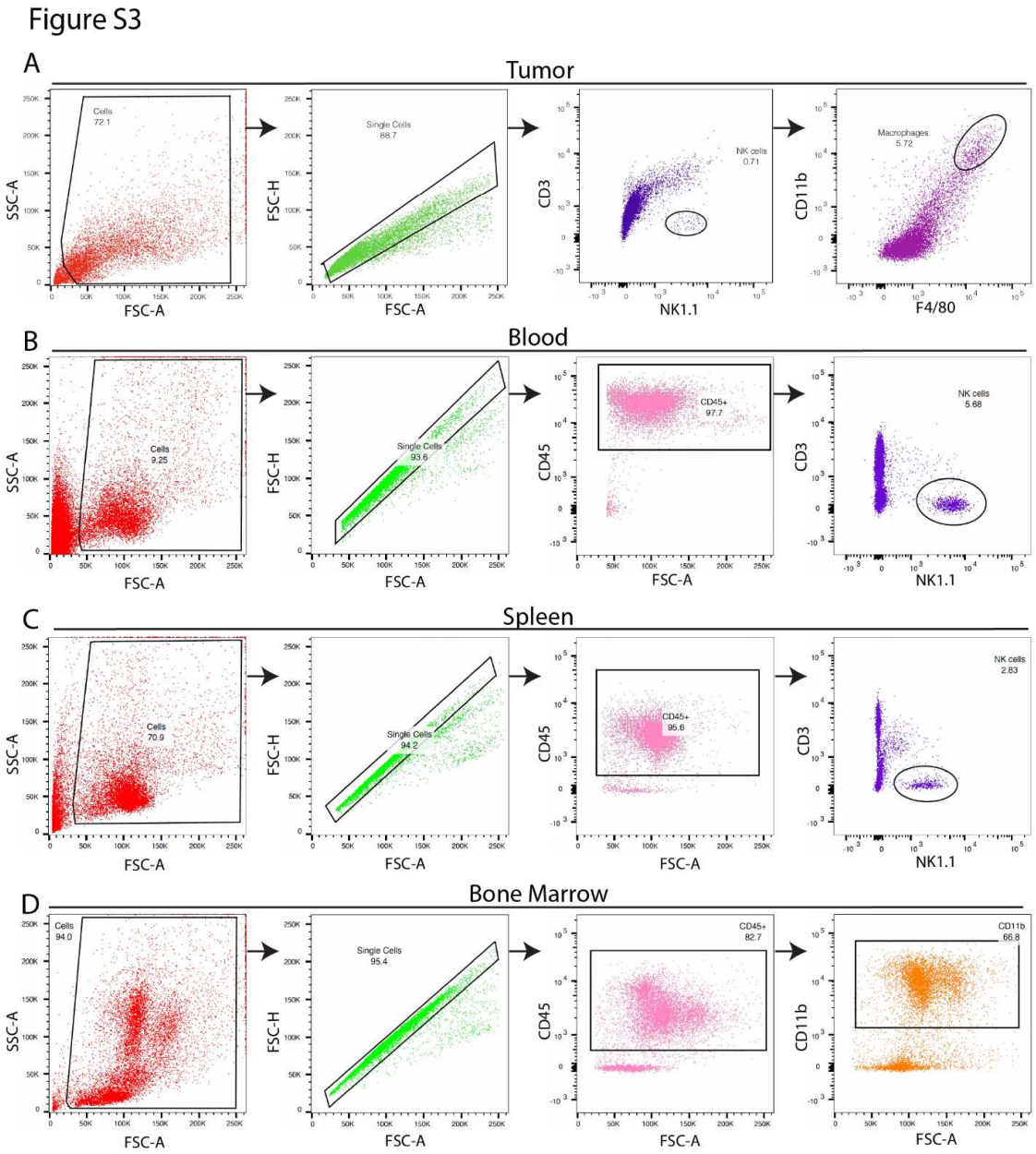

Figure S3. Flow cytometry analysis gating strategies.

(A) Gating strategies for flow analysis of tumor-infiltrating NK cells and TAMs. (B) Gating strategies for flow analysis of blood NK cells. (C) Gating strategies for flow analysis of splenic NK cells. (D) Gating strategies for flow analysis of bone marrow CD11b+ cells.

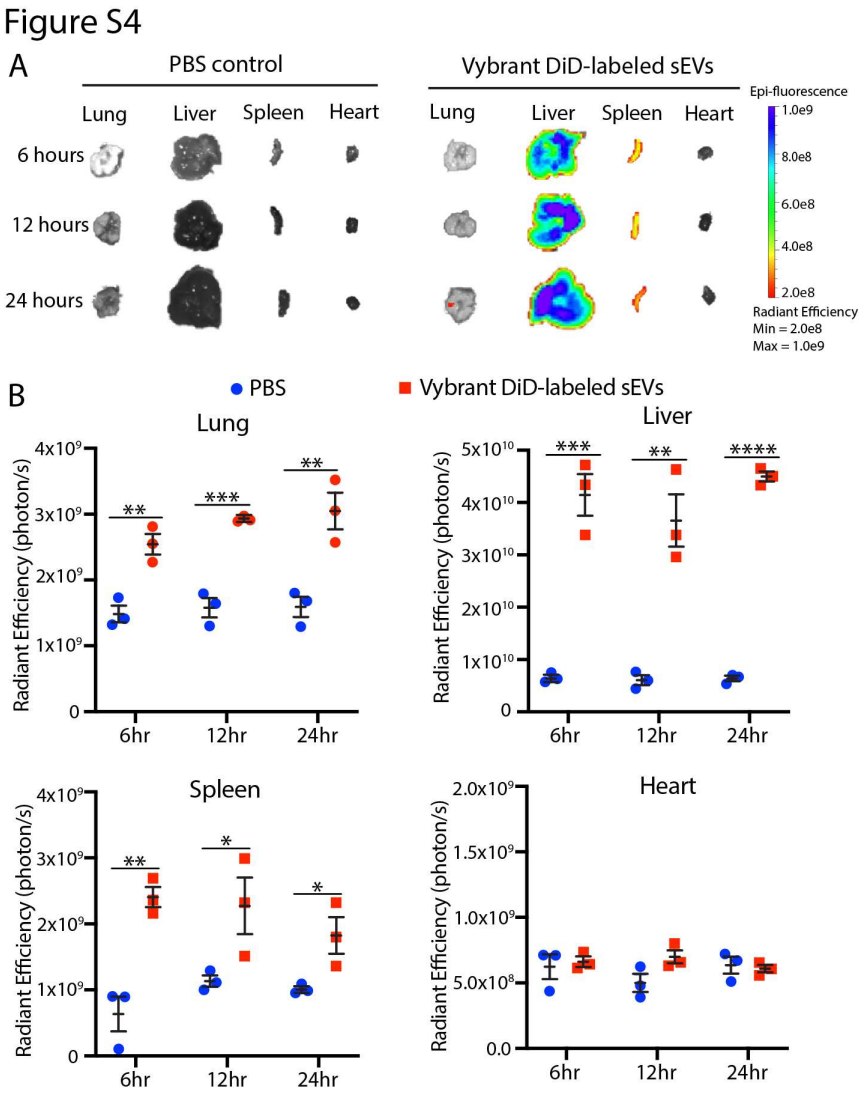

Figure S4. Neuroblastoma-derived sEVs primarily localize to the liver, spleen, and lung *in vivo*.

(A) Whole-organ fluorescence measured using the IVIS Imaging System at 6-, 12- and 24-h following tail vein injection of PBS or 20µg Vybrant DiD-labeled 9464D-GD2 sEVs in C57Bl/6 mice. (B) Quantification of whole-organ fluorescence intensities for lung, liver, spleen and heart. Mean ± SEM, n=3. Student's t-test. *, $p < 0.05$; **, $p < 0.01$; ***, $p < 0.001$; ****, $p < 0.0001$.

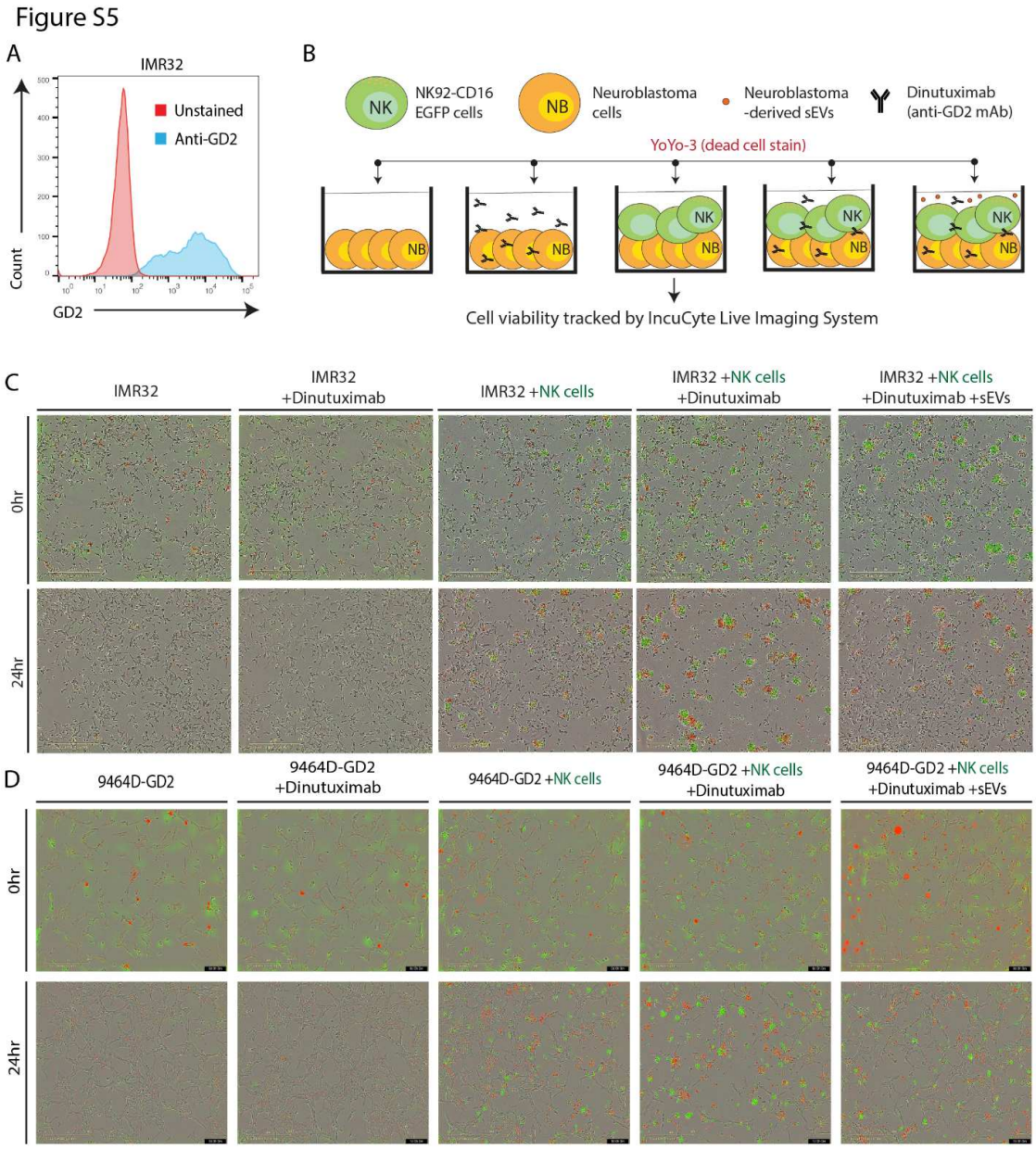

Figure S5. Human neuroblastoma cells express cell surface GD2 and are sensitive to dinutuximab-induced NK cell-mediated ADCC.
(A) Flow cytometry analysis of cell surface GD2 expression level in IMR32 human neuroblastoma cells. (B) Experimental design for *in vitro* NK-cell-mediated ADCC assay. (C-D) Representative images of IMR32 (C) and 9464D-GD2 (D) cells treated in the presence or absence of NK92CD16-EGFP cells (NK cells) and sEVs. Images obtained using the IncuCyte

Live-Cell Analysis System in the presence of the cell impermeant nucleic acid stain YOYO-3 (red). Scale bar, 400 µm.

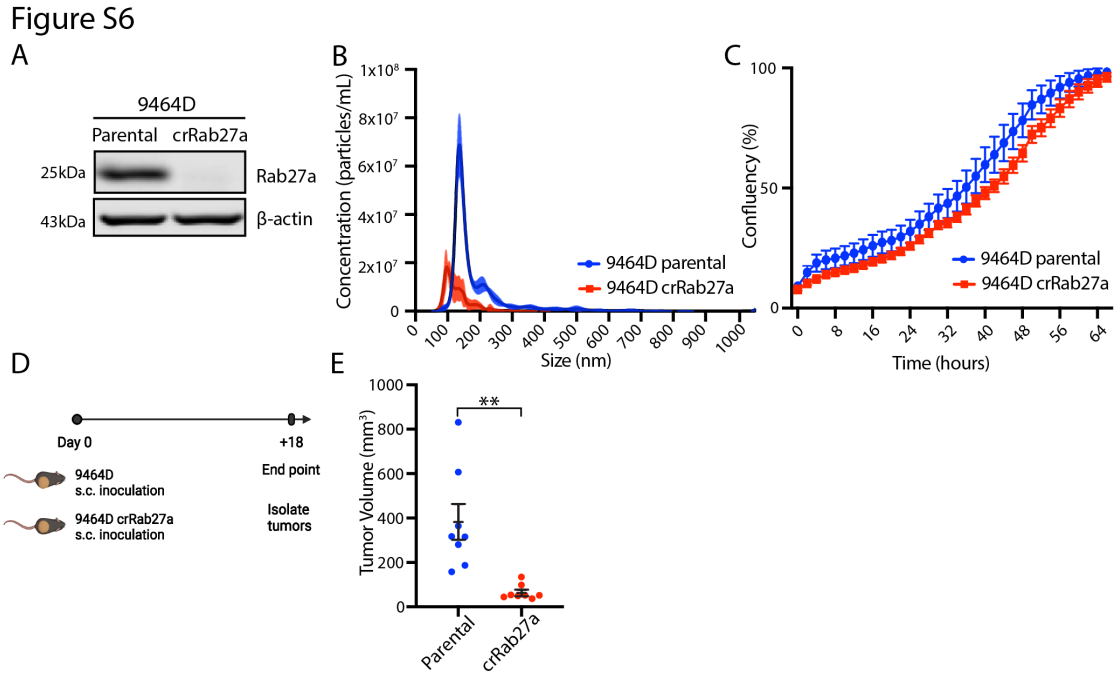

Figure S6. Loss of *Rab27a* inhibits 9464D tumor growth *in vivo*.
(A) Immunoblot of Rab27a in whole cell lysate of parental 9464D cells and 9464D crRab27a cells. All lanes loaded with equal amount of protein. (B) Representative size distribution and concentration of sEVs isolated from 9464D cells and 9464D crRab27a cells quantified by NTA. (C) Proliferation of 9464D cells and 9464D crRab27a cells quantified using the IncuCyte S3 LiveCell Analysis System. Mean ± SEM, n = 6. (D) Experimental design for E (created with BioRender.com). C57Bl/6 mice were subcutaneously inoculated with 1 x10^6 9464D cells or 4 x10^6 9464D crRab27a cells. On day 18, tumors were harvested for analysis. (E) Quantification of 9464D and 9464D crRab27a tumor volume on day 18. Mean ± SEM, n = 8. Student's t-test. **, $p < 0.01$.

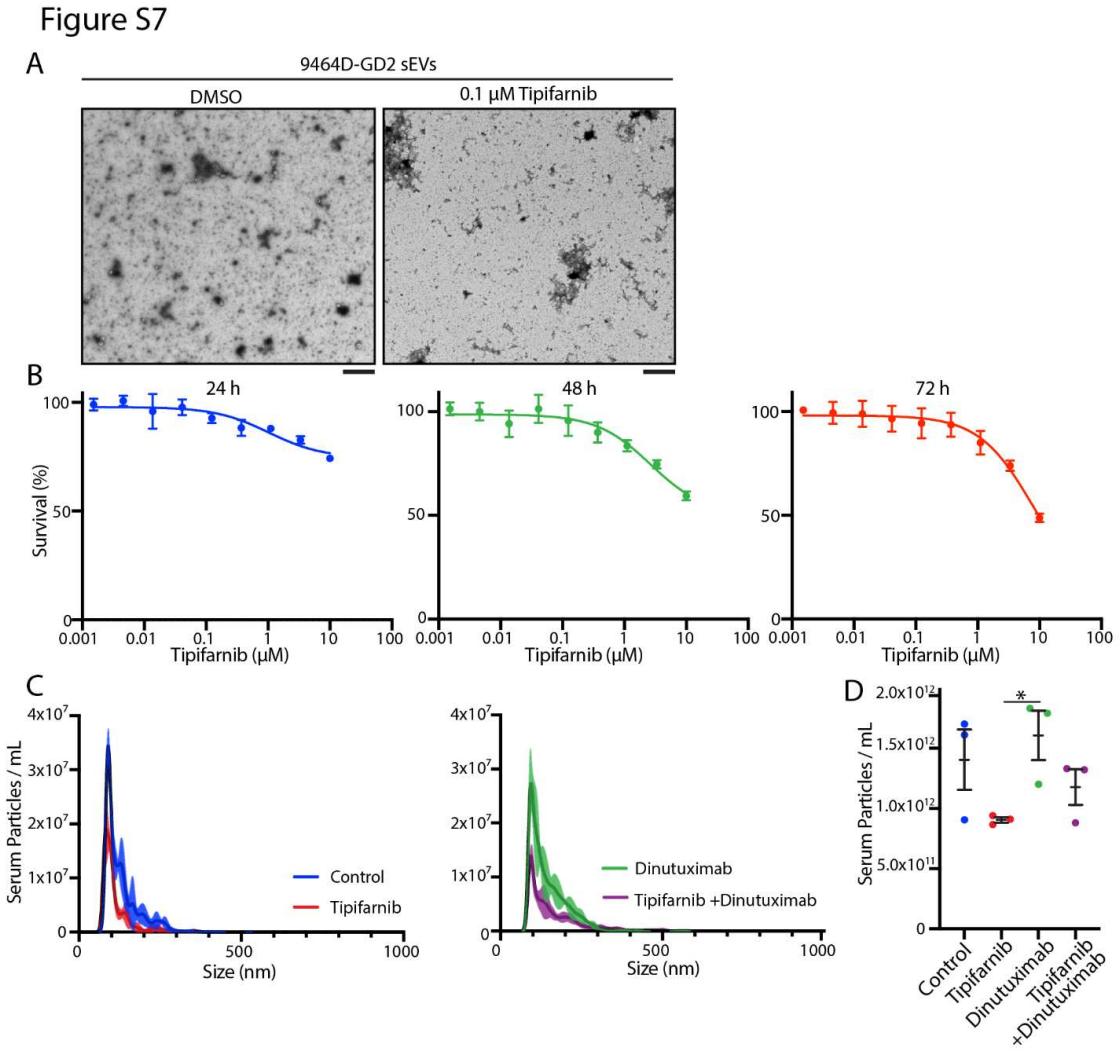

Figure S7. Tipifarnib suppresses sEV secretion both *in vitro* and *in vivo.*

(A) Representative electron microscopy images of sEVs isolated from 9464D-GD2 cells treated with DMSO or 0.1 μM tipifarnib for 48 hours. Scale bar, 1 μm. (B) Cell viability of 9464D cells treated with indicated concentrations of tipifarnib at 24-, 48-, and 72-h. Mean ± SD, n = 6. (C) NTA analysis serum sEV size distribution and concentration isolated from mice treated as described in Figure 4D on day 24. (D) Quantification of serum sEV concentration by NTA. Serum sEVs isolated from mice treated as described in Figure 4D on day 24. Mean ± SEM, n = 3. Student's t-test. *, $p < 0.05$.